USE OF OCEAN MODELS TO VALIDATE SURFACE FLUX PARAMETRIZATIONS

David L.T. Anderson
Department of Physics
Oxford, U.K.

David J. Carrington
Meteorological Office
Bracknell, U.K.

Abstract: To verify Ocean models, it is necessary to run them with prescribed forcing, such as the momentum flux and a parametrisation for the heat flux. This is illustrated in section 2 where the ability of ocean models to simulate the seasonal cycle and the interannual variability of the tropical Pacific is demonstrated. In contrast, ocean models can also be used to intercompare or validate different flux products. This is illustrated in section 3 for the case of the UKMO and ECMWF momentum fluxes and in section 4 for the heat fluxes from the ECMWF model in analysis and climate simulation modes.

1 INTRODUCTION

Ocean modelling differs from atmospheric modelling in one major respect. The important external forcing parameters in atmospheric modelling, viz the solar constant and sea surface temperature (SST), are relatively well known. In contrast, the major forcings for the ocean, the surface fluxes of momentum, heat and fresh water are relatively poorly known. If ocean models were accurate then they could be used to quality control the fluxes from atmospheric models, by using the fluxes to force ocean models and then comparing the quality of the resulting output from the ocean model with ocean measurements. Models which can be used for this purpose are models of the high frequency barotropic response, which depends only on the momentum flux or models of the slower baroclinic response which require inputs of momentum and heat. Ideally they require the fresh water flux too, but not all models have active salinity. In this paper, attention will be given to the baroclinic response. As in many fields, a somewhat circular or iterative approach is needed whereby ocean models are used to verify fluxes and fluxes are in turn used to verify ocean models.

Before considering applications to test the model response to different forcings, consideration will be given to different tests which have been made to verify ocean models, with the purpose of highlighting some of the potential errors in ocean models. Two types of test will be illustrated. The first is of the ability of ocean models to simulate the seasonal cycle, the second is of their ability to reproduce interannual variability in the tropical Pacific. In section 3 consideration will be given to model runs using momentum fluxes from the ECMWF and UKMO analysis suites. In section 4 the use of heat and momentum fluxes, not only from the ECMWF analysis suite but also from short climate integrations of the ECMWF model will be discussed.

2 VALIDATION OF OCEAN MODELS

2.1 The Seasonal Cycle

One might expect that the climatological seasonal cycle of wind stress τ, and even possibly heat flux would be reasonably well known, given that measurements have been collected for many years. Since the objective of this section is to validate ocean models, then the best possible forcing fields are required. For the momentum flux the most widely used is that due to Hellerman and Rosenstein (HR) (1983). Unfortunately, this is not as accurate as one would like and a perception has arisen in the ocean modelling community that in the tropical Pacific, Hellerman stresses are too large. By how much is a debatable issue. A model intercomparison has been initiated by the TOGA-Numerical Experimentation Group (Stockdale *et al.* 1993) to intercompare models of the seasonal cycle. They chose as momentum flux 0.75 times that of HR.

If an ocean model is forced with a wind stress then it will come to some equilibrium with that wind field. If the stresses are in error, then the currents will be in error but still a reasonable statistical equilibrium will be obtained. This is not true in the case of heat flux, however. If too much heat is applied to the ocean, then SST will continue to rise. No sensible equilibrium will be obtained. This can be both useful and troublesome. In section 4, we will use this to advantage to test ECMWF fluxes, but for now it poses a problem. No sensible extended (few year) integrations are possible using a prescribed heat flux. For that reason the heat flux used in the intercomparison experiments was of the form

$$Q = Q_{clim} + \lambda(T - T_{clim}) \qquad 2.1$$

where Q_{clim}, is an estimated climatological heat flux. The one chosen was that of Oberhuber (1988). The degree of disagreement between this and other climatologies is generally 20~50 W/m^2, comparable to ~30% of mean climatological values, indicating that the uncertainty is considerable, even for the climatological seasonal cycle. The $\lambda(T - T_{clim})$ term in (2.1) is a negative feed back term restoring the value of T towards the observed climatological seasonal cycle of SST. The value of λ, obtained from Oberhuber, varies geographically but is typically 40W/m^2/K. The specification (2.1) is equivalent to a simple atmospheric model.

Figs. 1a,b,c,d show the SST error in March from four integrations to give some idea of the spread of error between ocean models. Where all models have the same error, one might anticipate that it arises from forcing error, though not necessarily locally. Error which varies from model to model is probably indicative of model error. The first three models are general circulation models which are well resolved in the vertical but with decreasing horizontal resolution, while the fourth shows a 2-layer model with moderate horizontal resolution.

The errors in the West Pacific are typically $1°C$, which implies the climatological heat fluxes are too high. The anomalous heat flux $\lambda(T - T_c)$ is ~ 30 W/m^2 but does not imply that if the climatology were reduced by this amount the ocean would reproduce the SST there accurately. Further east, along the equator almost all models are too cold. This is most accute at the time of the spring relaxation when the model fails to warm as much as reality. This could result from an overstrong wind stress as cold water in the east Pacific arises as a result of a pressure gradient balance with the wind stress. If the stress were too strong then the water in the east would be too cold. However, it is hard to argue that the stress used is too strong, as reducing HR by 25% is a substantial reduction. Further, the error varies from model to model and is generally least in the well resolved models. The errors along the eastern boundary are quite large. The nature of the error varies from model to model, but is qualitively similar in all. The cause is unknown.

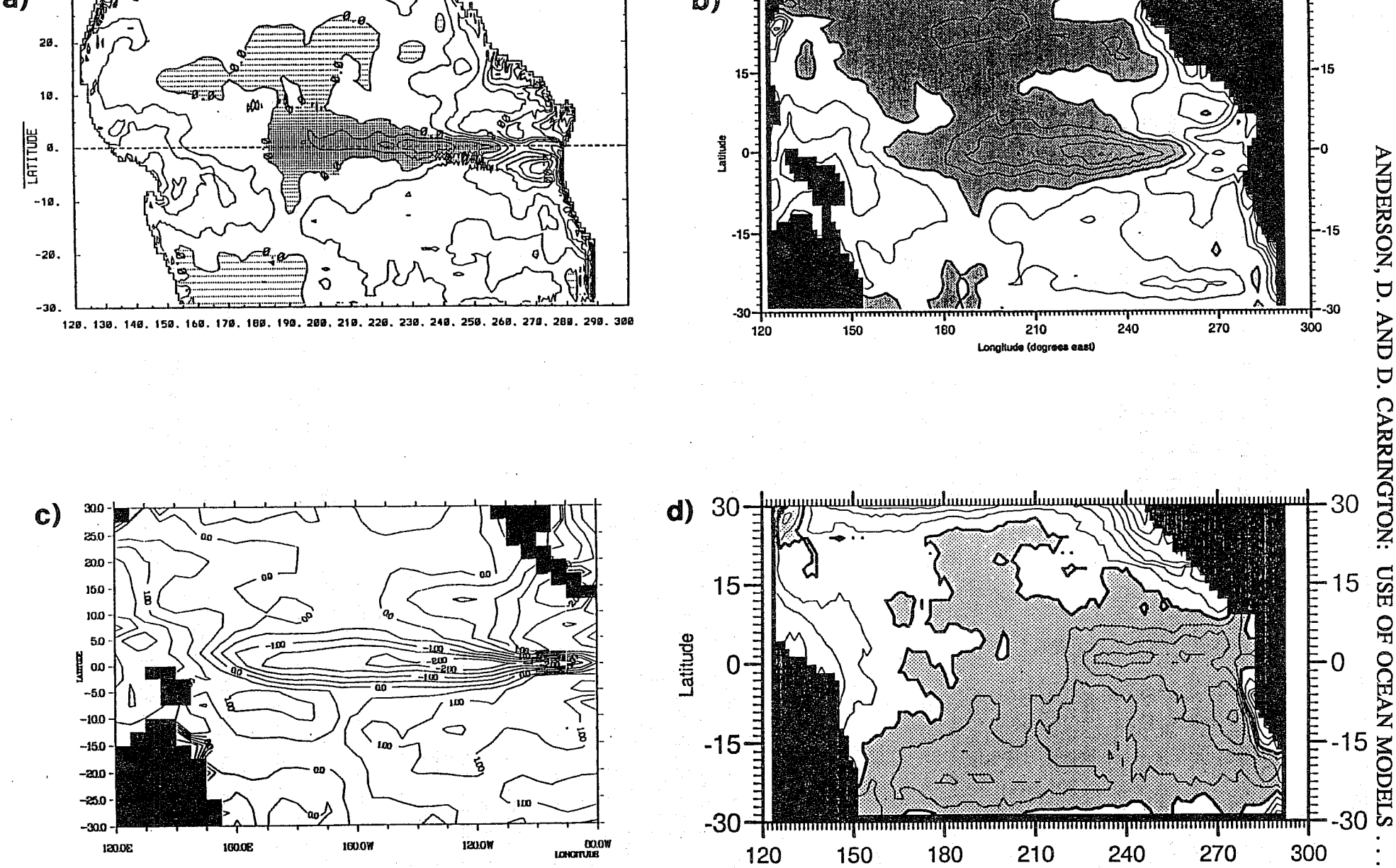

Figure 1: SST errors in four simulations of the seasonal cycle. In a) the equatorial resolution is $\frac{1}{3}°$x$\frac{3}{4}°$, in b) $\frac{1}{2}°$x$\frac{3}{2}°$, in c) $\frac{1}{2}°$x5° while in the vertical resolution there are 21, 16 and 17 levels. In d) the horizontal resolution is 1.5°x1.5° but there are only two layers in the vertical. Case a) is the LODYC model (Delecluse), b is the Oxford model based on the Cox Bryan GCM model (Stockdale), c is from MPI (latif) and d is from Oxford based on the Anderson model (Balmaseda).

However, for the best resolved models, the size of the errors can largely be accounted for by errors in the forcing and therefore cannot be verified further, at least not on their ability to reproduce the seasonal cycle. On the other hand, several of the models have errors which lie outside what can be accounted for by present estimates of error in the forcing fields. In these cases, model errors do clearly exist. The magnitude of the error is not fully quantified, however, as the seasonal cycle of SST based on multiyear runs using real forcing is not the same as that obtained if the forcing is averaged first. There is a rectification effect, of the order of 0.5°C to 1.0°C which varies from model to model, both in magnitude and location.

2.2 Simulation of Interannual Variability

A second test which might be applied, is to force ocean models with the perceived forcing fields over the last 30 years or so. (Ideally this should be longer, but ocean wind fields only go back this long and even then are of dubious quality in the earlier years). There are no corresponding fields of interannual heat flux, and it might appear that models can not be tested in this way. However, in the Pacific much of the interannual variability in SST arises from variations in the wind and not in heat flux. In fact, the approximation that the atmosphere is always acting to damp anomalies through the heat flux is remarkably good. It probably does not apply always and it is certainly not true everywhere that we can produce interannual variations just from the wind.

Fig. 2b,c,d shows the SST observed at the three regions EQ1,2,3 shown in Fig. 2a over the period 1961-1991, from a model used at Oxford (Balmaseda and Anderson). Other models will produce slightly different simulations (see later). The model does reasonably well in regions EQ1 and 2, but less well in EQ3. Other models have been tested. The correlation of this and other models with the observed SST is shown in Table 1. The correlation is generally quite good, but varies between model. The models do better in the central east Pacific than in the west Pacific which suggests that some of the error is model-based and could be reduced if we took the best features of all models. Additional model intercomparison is considered by Miller et al 1992.

Table 1 Correlations for the regions EQ1, EQ2, EQ3 between four Models and the Observed SST

	A	B	C	D
EQ1	0.69	0.69	0.52	0.51
EQ2	0.80	0.77	0.78	0.67
EQ3	-	0.428	0.53	0.344

A and B are the 2-layer and GCM models, respectively, described in the previous section. Model C is a perturbation model and D a 2-layer model with higher resolution than A but with different thermodynamics. All models are in use at Oxford by Anderson, Allen, Balmaseda, Davey, Lawrence and Wu.

The conclusion from this section is that ocean models can simulate interannual variability in the tropical Pacific reasonably well, that the wind stress forcing does contain the germ of real interannual variability (see also section 5) and that to some useful degree the atmosphere acts as a negative feedback in the tropical Pacific.

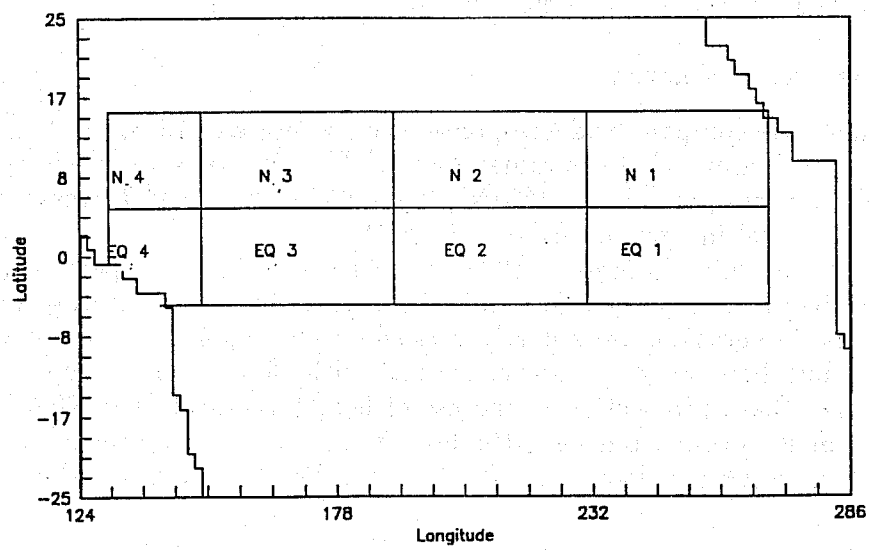

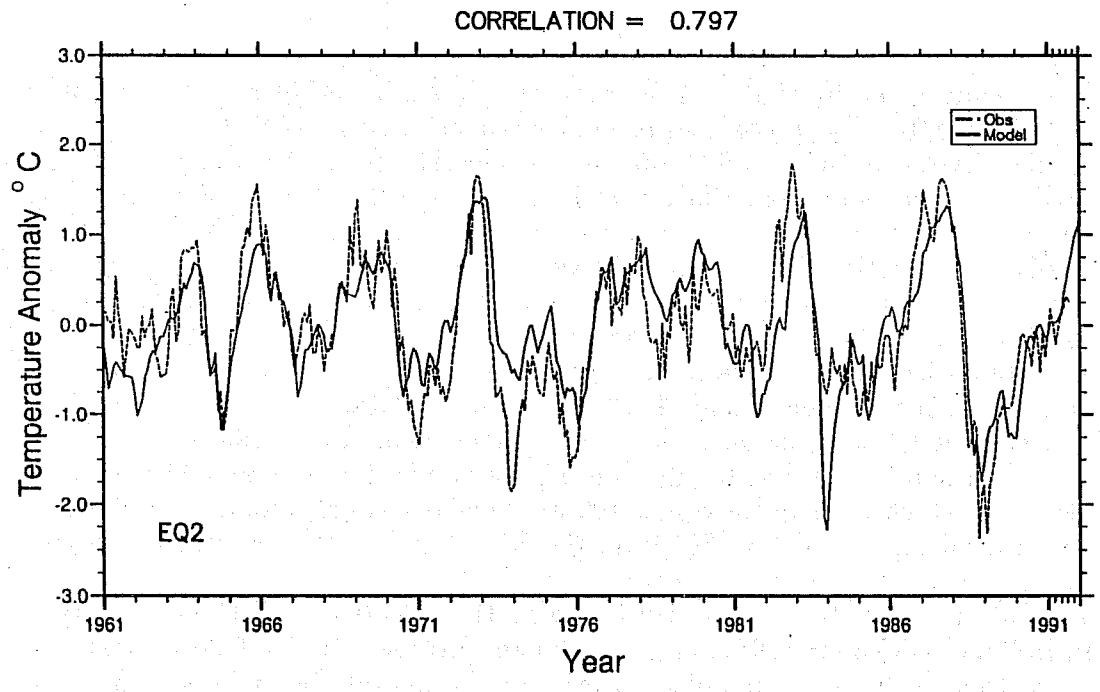

Figure 2: SST anomalies over a 30 year period for the model of Fig. 1d. Also shown are the observed anomalies.

3 SIMULATIONS USING ECMWF AND UKMO SURFACE MOMENTUM FLUXES

3.1 Comparison of Currents

In this section we will compare model response when we use HR, ECMWF and UKMO surface stresses to force a model of the Indian Ocean. The integration periods are 1987/1988 using ECMWF stresses (experiment INDN), 1987-1990 using UKMO stresses (experiment INDG) and a seasonal integration using HR (IND1).

A period of particular interest is 1987 and 1988 as this was a period when rainfall over India was below average in 1987 (an El Nino year) but above average in 1988 (a La Nina year). The integrations were partly carried out to examine interannual differences in the model, but here we are more concerned with differences arising as a result of different forcings. Later, in section 4, the use of heat fluxes from the ECMWF analyses is considered but for present purposes the heat flux is obtained by relaxing SST back to climatological values with a time-scale of $\sim$ 50 days. The heat fluxes in these integrations are

$$Q = Q_{clim} + \lambda(T - T_c^*)$$

$$S = S_{clim} + \lambda(S - S_c^*)$$

with Q_{clim} being given by that of Esbenssen and Kushnir (1981) and λ has a uniform value of $35\mathrm{W/m^2/K}$. This probably prevents a proper analysis of SST variability, since, in the Indian Ocean, changes in SST may be less closely tied to variations in thermocline depth and more dependent on surface heat fluxes than in the Pacific, where the negative feedback approach appears to work quite well (section 2). It does, however, allow an analysis of the circulation field. Ideally one would like to compare the model output with observations, but current measurements for the 1987–1990 period in the Indian Ocean are almost totally lacking. Therefore interannual variations in currents are examined (section 2) but with little verification of their correctness. A comparison has been made between model dynamic height and GEOSAT altimeter data.

The ocean model used has been described in Anderson *et al.*, (1991) and so will not be discussed in detail here, but briefly, it is a general circulation model with 16 levels in the vertical, of which 7 are in the upper 100 m. The latitudinal resolution varies from $\frac{1}{3}^\circ$ in the equatorial region to 1° at 30° from the equator while the longitudinal resolution varies from $\frac{1}{2}^\circ$ near the western boundary to $1\frac{1}{2}^\circ$ in the east.

Details of the way stresses are calculated in the UKMO and ECMWF models are given in Bell and Dickinson (1987) and Blondin and Bottger (1987). Operational forecast models are frequently being modified. However, the period chosen was a rather quiet one in this regard with no significant changes to the UKMO system, during this time. Likewise at ECMWF, large changes were made in 1986 and 1989 but the years 1987 and 1988 were relatively stable.

Analysed wind fields from operational weather forecast centres can differ markedly from published climatologies. This is illustrated in Fig. 3, in which the average seasonal cycle of zonal wind stress on the equator based on the 4 years 1987–1990 at (a) 55°E, taken as representative of the western region, and (b) 73°E, taken as representative of the central eastern region, are plotted (solid curve) for comparison with the seasonal cycle of zonal stress from HR shown by the dashed curve. The longitudes 55°E and 73°E correspond to two sites where most oceanographic data for the Indian ocean have been collected (see Leetmaa and Stommel 1980 who collected two years of Spring data at 55°E and Knox 1976 who collected $2\frac{1}{2}$ years of data at Gan, 73°E).

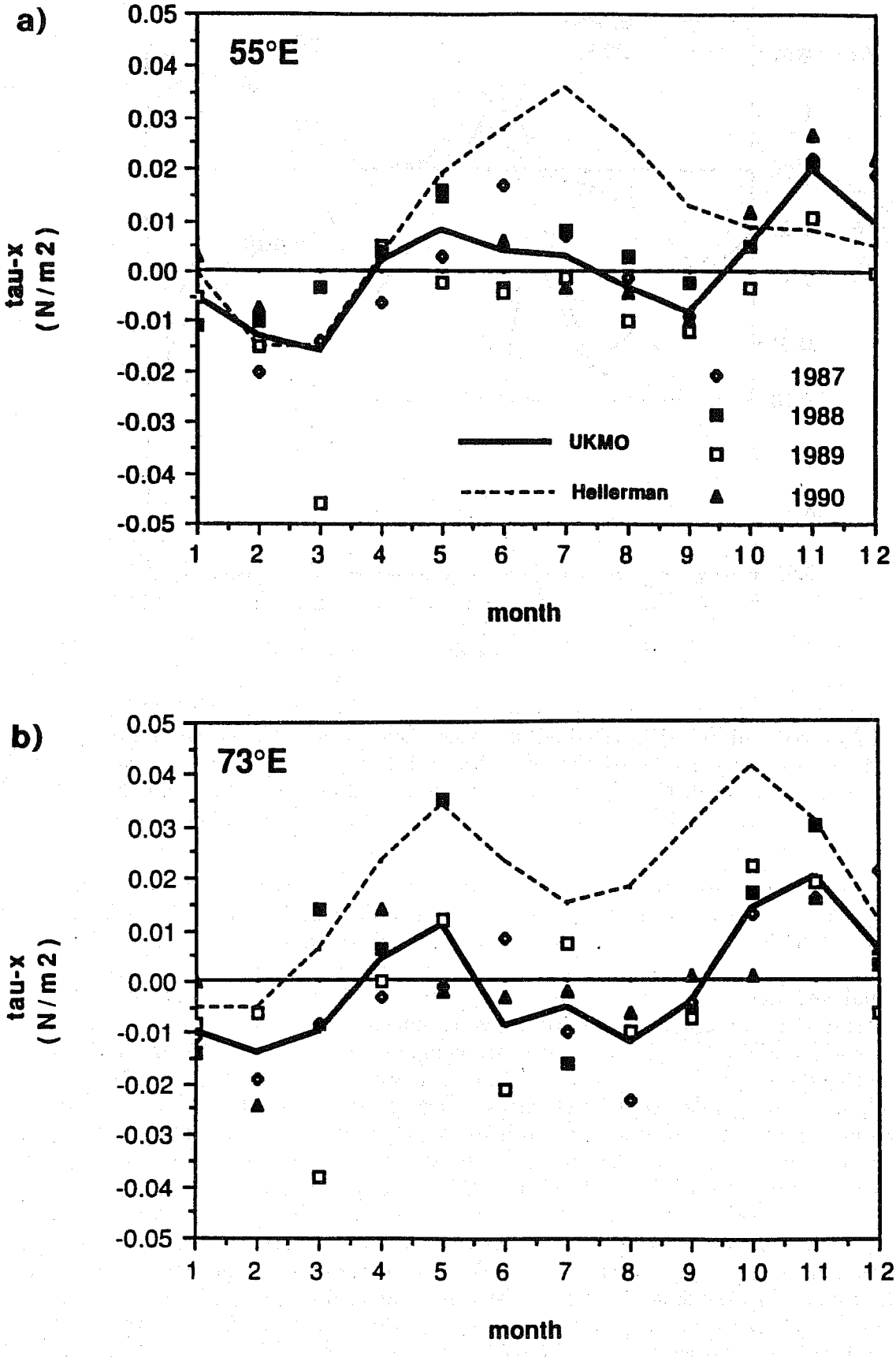

Figure 3: Plot of the seasonal cycle of zonal wind from the UKMO analyses (solid curve), averaged over the 4 years 1987–1990 for (a) 55°E and (b) 73°E. For comparison, the seasonal cycle from Hellerman and Rosenstein (1983) is shown (dashed curve). There is a noticeable bias between the two wind products, with HR approximately 0.01 to 0.02 Nm^{-2} stronger on average. In order to show the range of interannual variability, the values for the individual years are also shown.

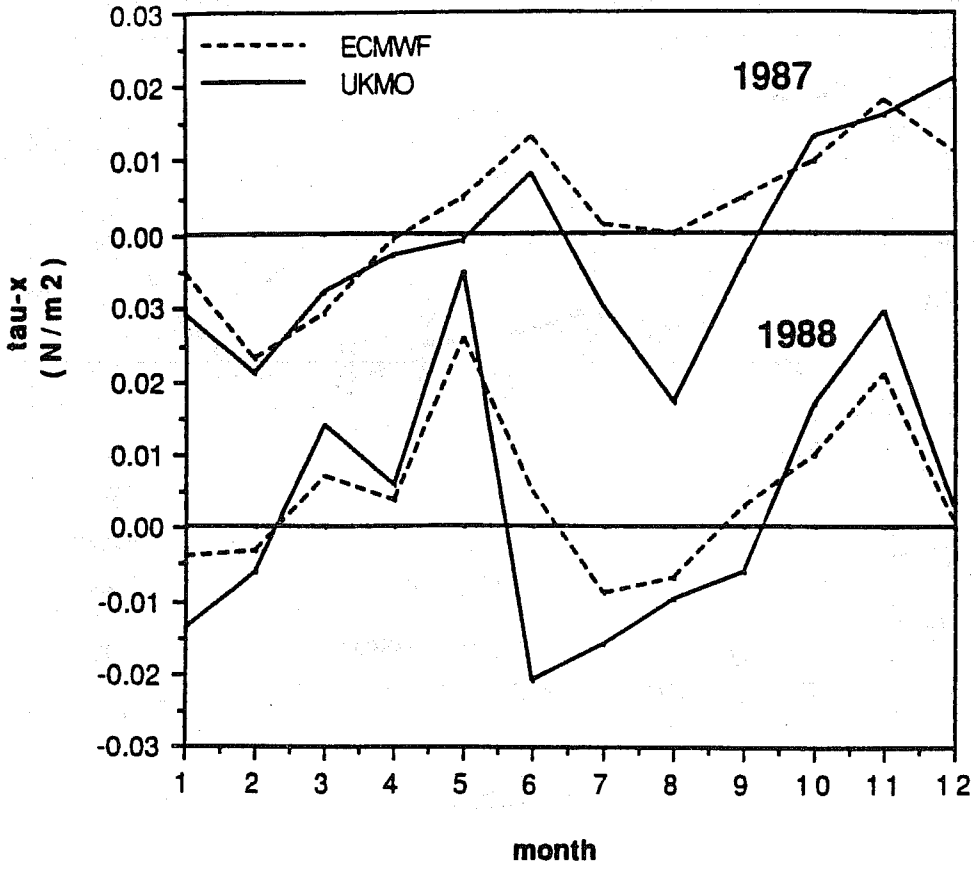

Figure 4: Plot of the monthly mean zonal wind stress for 1987 and 1988 at 73°E from the UKMO (solid) and ECMWF (dashed) analyses. Both show similar interannual variations, with differences of typically less than 0.01 Nm^{-2}, but in Aug 87 and June 88 the differences are larger, up to 0.025 Nm^{-2}. The UKMO shows larger variability than ECMWF and shows stronger westward stresses, particularly in Northern Hemisphere summer.

At both locations, there are substantial differences between the forcing fields; for example the HR stresses are considerably stronger than the UKMO stresses, on average by about 0.02 Nm^{-2}. This variation is comparable to the amplitude of the seasonal cycle and is significant in terms of the equatorial ocean currents it can drive. Also shown are the analysed values for the individual years 1987–90. At both locations, the HR stresses lie outside the interannual variability range for much of the year.

The ECMWF and UKMO stresses are compared for the years 87 and 88 in Fig. 4. Again there are large differences. For example, in June and July 1987 the ECMWF stresses are almost zero, while the UKMO stresses are greater than $0.02N/M^{-2}$ to the west. Examination of Fig. 3 shows that the interannual range is approximately $\pm 0.015NM^{-2}$ and so the inter-analysis differences are almost as large as the interannual differences. How can one verify ocean models with such large uncertainties?

In Fig. 5 the mean seasonal cycle of surface zonal currents is plotted for the experiment forced by the UK Met. Office wind stresses, denoted INDG. At 55°E, the currents show a marked semi-annual cycle, with a mean which is *westward*, even though the annual wind stress is not. In May and November, there are eastward currents of strength 25 cm s^{-1} and 40 cm s^{-1}, corresponding to the Wyrtki Jet (Wyrtki, 1973). This is stronger further to the east, as can be seen in Fig. 4 for 73°E, where the Spring and Autumn speeds reach 50 cms^{-1} and 60 cms^{-1}. At this longitude the currents for INDG have an annual mean close to zero. The currents from IND1 are also shown for comparison. At both 55°E and 73°E, the currents are more eastward in IND1, consistent with the stronger eastward wind stresses in the HR analysis.

The average seasonal cycle of zonal currents at 113 m (representative of the under-

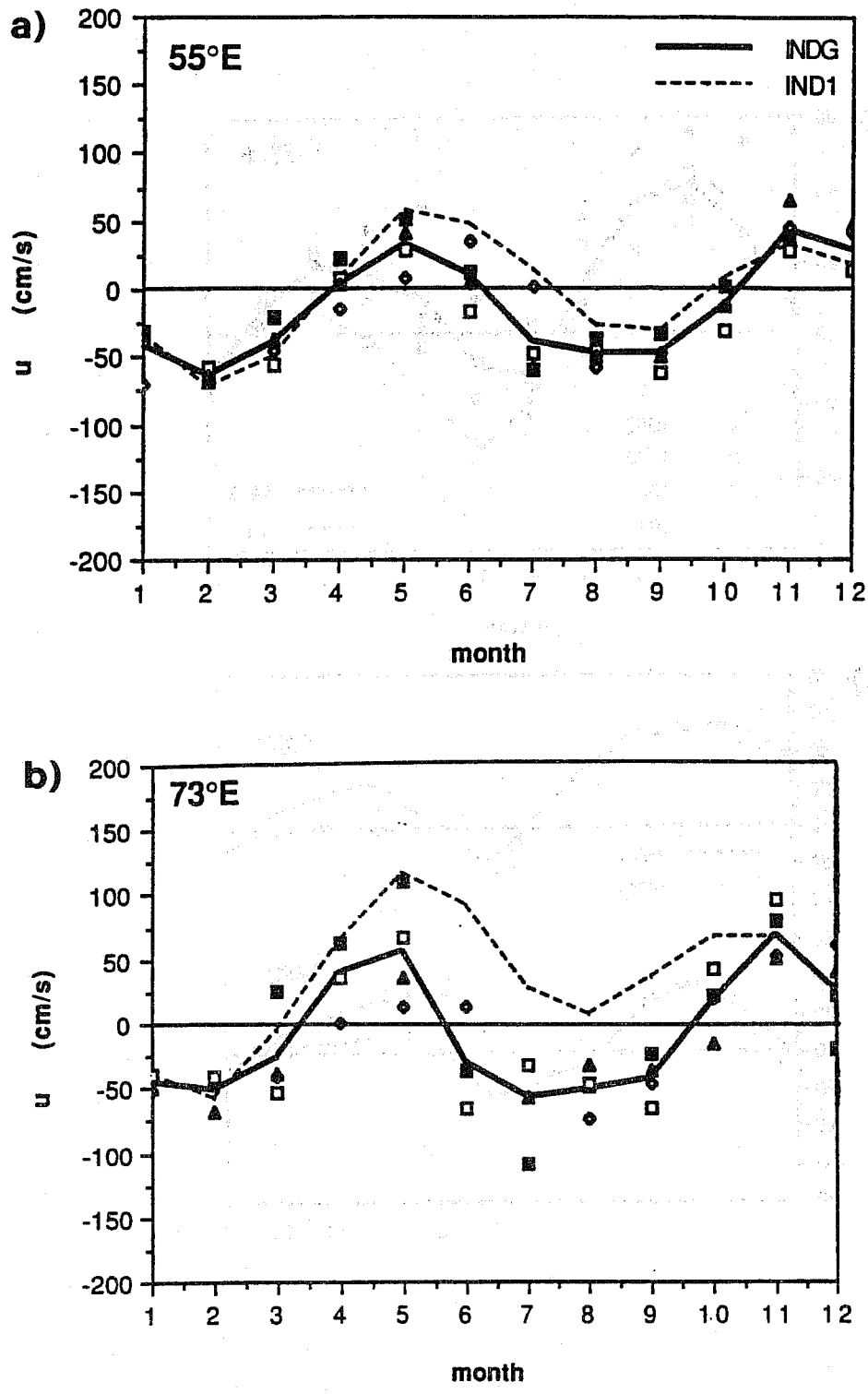

Figure 5: Plot of the seasonal cycle of surface zonal currents from INDG (solid) and for IND1 (dashed), the former experiment corresponding to forcing by UK Met Office stresses and the latter to Hellerman and Rosenstein forcing, for (a) 55°E and (b) 73°E. The currents in IND1 are more strongly eastward than those in INDG consistent with the stronger eastward stresses of IND1. The currents for each month in the period 1987-90 are also shown, to indicate the range of interannual variability. This is typically around 50 cm/s, but can be as large as 100 cm/s in May and as small as 10 cm/s in January.

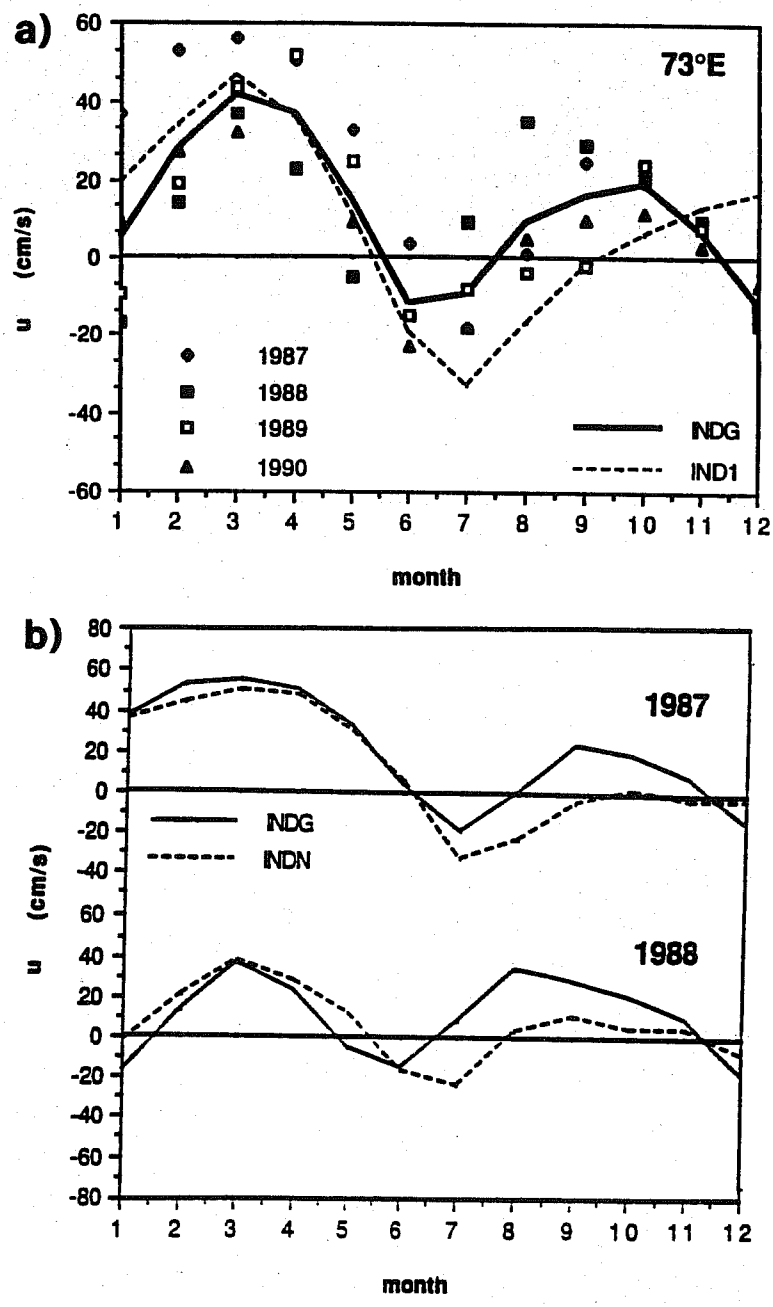

Figure 6: a) The 4-year average seasonal cycle of zonal currents at 113 m at 73°E from INDG, compared with the seasonal cycle from IND1. INDG shows a marked semi-annual response, but that in IND1 is annual. b). Plot of zonal currents at 113 m at 73°E for INDG and INDN for 1987 and 1988. The currents obtained using UKMO stresses show stronger eastward flow than the currents obtained using ECMWF or HR stresses. Both INDG and INDN show a semi-annual response, contrary to IND1 but consistent with observations shown in fig. 7.

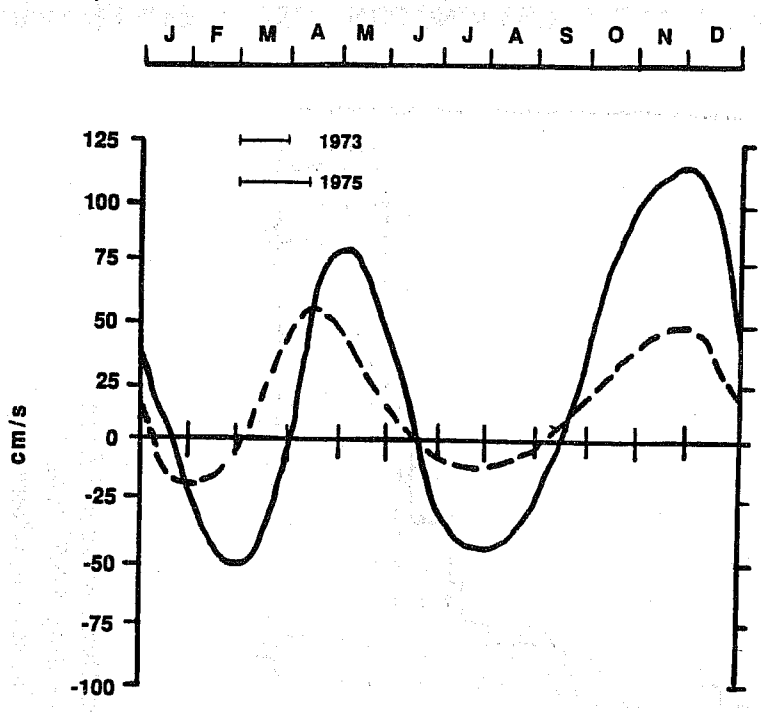

Figure 7: Seasonal composite of currents from 90 profiles at Gan (73°E) for the period January 1973–June 1975 (Knox, 1976). The solid line is for currents in the mixed layer ; dashed line for the currents at the 20°C level. The timing of the undercurrent is indicated in upper left of the diagram when known; it is earlier in INDG than in these observations. From Reverdin 1987. The timing of the undercurrent is earlier in INDG than in Fig. 6. There is a marked semi-annual response both at the surface and at ~100m, consistent with INDG but not IND1.

current depth) together with the interannual variations in undercurrent strength at 73°E are plotted in Fig. 6. Whereas there were large differences in the surface currents between IND1 and INDG, these differences are somewhat smaller at undercurrent depth particularly in the first 6 months of the year despite the large differences in wind stress: it is in the latter half of the year that the currents are most different. Comparison with Fig. 3 shows that although the annual mean wind is not strongly eastwards in INDG, the mean current at 113 m *is*, much more so than in IND1 even though the wind is more strongly eastward in the latter. This results from the following dynamics. When the ocean is in steady state both eastward and westward winds will give rise to eastward flow at undercurrent depth, albeit for different reasons. The ocean response is not just related to the local wind: it also depends on remote forcing via Kelvin and planetary waves. In the case of a westward wind stress, the undercurrent may be established non-locally by the development of a pressure gradient against the western boundary. The stronger the westward surface stress, the stronger the eastward undercurrent. On the other hand, an eastward wind stress will drive an eastward surface flow, which can be transmitted to the subsurface by local vertical advection and mixing. A pressure gradient may be established of such a sign as to retard the eastward flow but may not be strong enough to offset the vertical exchange of momentum, resulting in a current which, at ~100 m, is still eastward although weaker than at the surface. It could be westward if the pressure gradient were stronger than the local vertical transfer terms but experience shows a strong asymmetry in the response to easterlies and westerlies. The winds change so rapidly in the Indian ocean, that the ocean is never in a state of equilibrium so the above pseudo-equilibrium arguments do not strictly apply but may nonetheless indicate why the ocean has a preference for eastward subsurface flow.

The mean (observed) seasonal cycle of currents at Gan is shown in Fig. 7. The INDG model undercurrent strengths are generally a little weaker than the observations, and

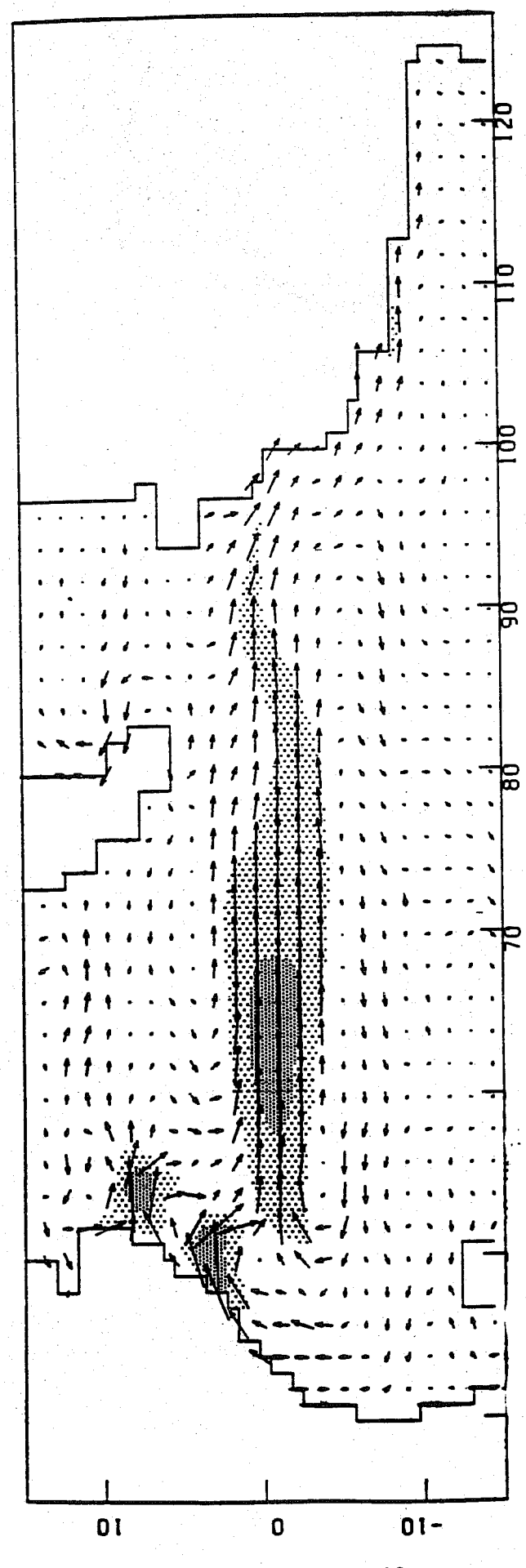

Figure 8: Plot of the vector difference in surface currents between those obtained from ECMWF forcing and those from UKMO forcing (INDN-INDG), for July 1988. The differences are largest in the Somali current region and in the equatorial region, where they reach almost 1 ms^{-1}. The currents along the Somali coast exhibit a more pronounced 2-gyre structure in INDN than in INDG. Light shading indicates current differences between 40 cms^{-1} and 80 cms s^{-1}. Heavy shading indicates current differences greater than 80 cm s^{-1}. The sign of the difference changes between May and June.

there are some phase differences, with model currents leading the observed by ~1 month. The surface currents also compare favourably, although the model currents are weaker. The biggest differences are in January when the model flow is westward but the observed flow is eastward. The currents in IND1 at both surface and undercurrent depth (not shown) agree with Fig. 6a less well than do those from INDG. In fact, because IND1 produces westward flow at ~100m in JJA, a *reverse* undercurrent exists, with surface eastward flow above a westward undercurrent. There is little evidence for such a flow although the data record is too short to exclude it as a possibility.

The currents from INDN are compared with INDG for the years 1987 and 1988 in Fig. 6b. Again the largest differences are in the second half of the year. Because of the shortness of the observation record and the fact that it is for a different period, it is hard to confirm that one product leads to better currents than another. This illustrates the difficulties in verifying momentum fluxes, even though as Fig. 8 shows the currents they produce are very different. One might think that SST would be a better quantity to verify against, since this is better observed. Fig. 9 shows the differences in SST between 1988 and 1987 for the two model runs INDG and INDN. Interannual variability in the Indian ocean is much smaller than in the Pacific so it is probably unlikely that a clear wind-driven signal would emerge and this was confirmed. There is some agreement between INDG and INDN in that the eastern equatorial region is warmer in July 1988 while the western area and Somali basin are cooler, but there is little agreement in detail or magnitude and neither agrees well with the CAC (Climate Analysis Centre) analyses, which themselves are not without error, of course. Qualitative comparison for other months supports the conclusion that the wind-driven variations in SST are not a good indicator of interannual variability in SST in the Indian ocean.

3.2 Comparison with GEOSAT and Levitus data

A comparison of the model simulations was made with GEOSAT and Levitus data. The GEOSAT surface deviations for various months and the differences in model dynamic height (calculated relative to 800 m), for the same month for INDG and INDN were compared. (In all cases the deviations are from an annual mean. In INDG, the same time period was used to produce the annual mean as for the GEOSAT data, but for INDN, the mean was the average of the years 1987 and 1988). There appeared to be some broad-scale agreement in the region north of the equator and even some correspondence between specific model features and GEOSAT in this region. In the Southern Hemisphere there is a large negative anomaly observed at 10°S, 90°E which is weakly present in INDG but not in INDN, although it is a dominant feature of the GEOSAT data. By constrast, a feature east of Madagascar is reproduced weakly in INDN but not in INDG. Quantitative agreement between the model runs and GEOSAT is generally poor. The differences between the modelled fields, are largest in the region of the Somali gyre (16 dyn cms) as a result of the different gyre structure and position induced in the INDG and INDN calculations referred to earlier. In a region around 5°S, differences between the model fields INDG and INDN exceed 10 dyn cms and there are several areas in which the differences are 4-6 dyn cms, not insignificant compared with interannual changes. Along the eastern boundaries the UKMO integration (INDG) has much stronger gradients than INDN.

In order to condense the large amount of data and to distinguish seasonal variability from interannual changes, a seasonal range, equal to the difference between the maximum and minimum monthly mean dynamic height in the mean seasonal cycle was calculated and is shown in Fig. 10b for Levitus and in Figs. 10c,d,e for experiments INDG, INDN, IND1. In the case of GEOSAT the surface topography was used (Fig. 10a). Comparison of the two observed fields 10a and 10b, shows some regions of agreement, especially the

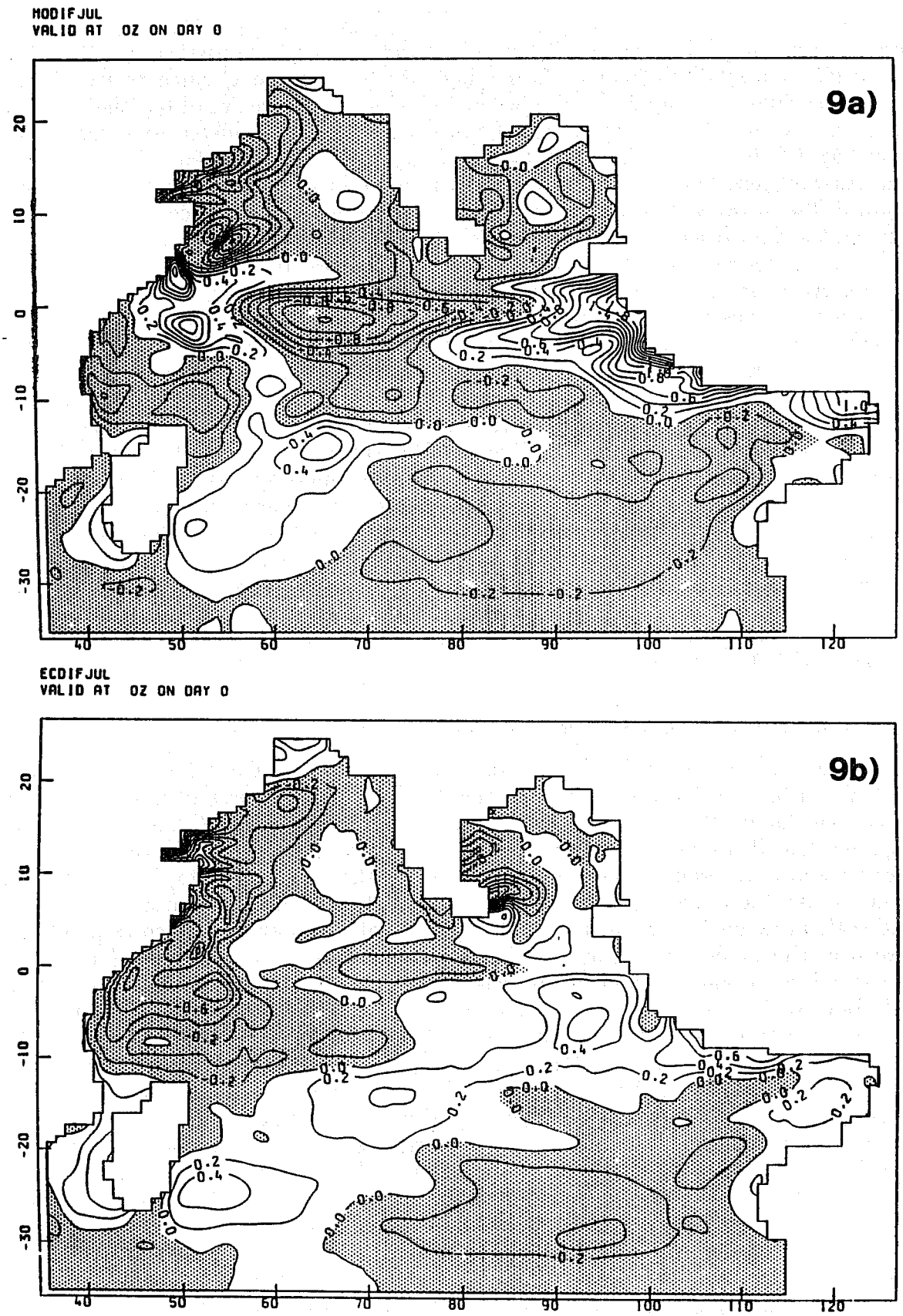

Figure 9: Plot of the SST differences between July 88 and July 87 for (a) INDG, (b) INDN and (c) The CAC analyses. The modelled differences in a are larger than in b or c, but neither a or b are good simulations of the observed differences shown in c.

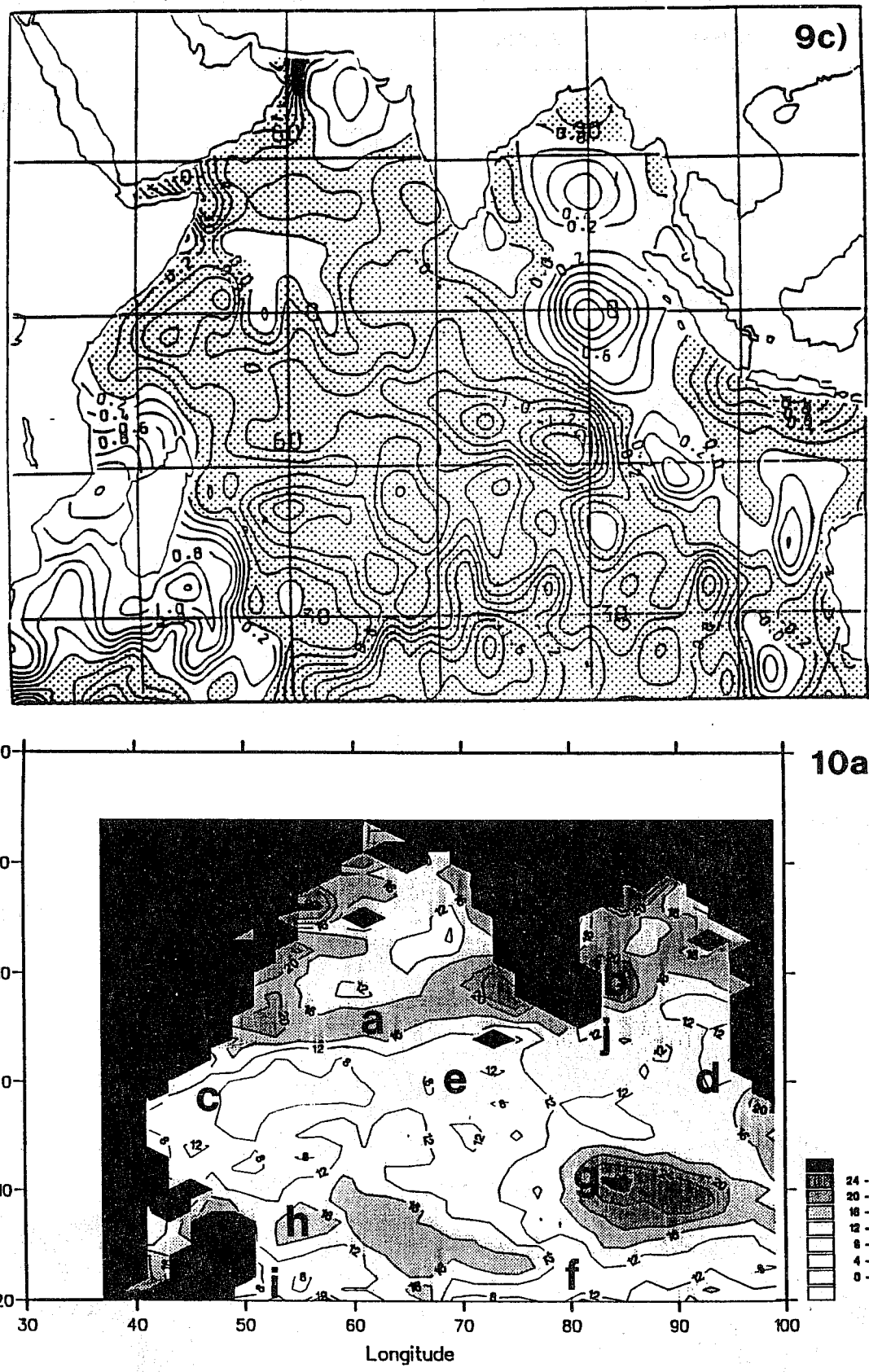

Figure 10: a) The seasonal range for surface topography observed by GEOSAT. b) Contours of the seasonal range in dynamic height (in dyn cm) for Levitus data. Solid lines at 20°S and 100°E correspond to the boundaries of the area of the GEOSAT data in a. c) As for b but for INDG. d) As for b but from the 2-year average seasonal cycle of INDN. e) As for b but from the seasonal integration using HR winds (Experiment IND1).

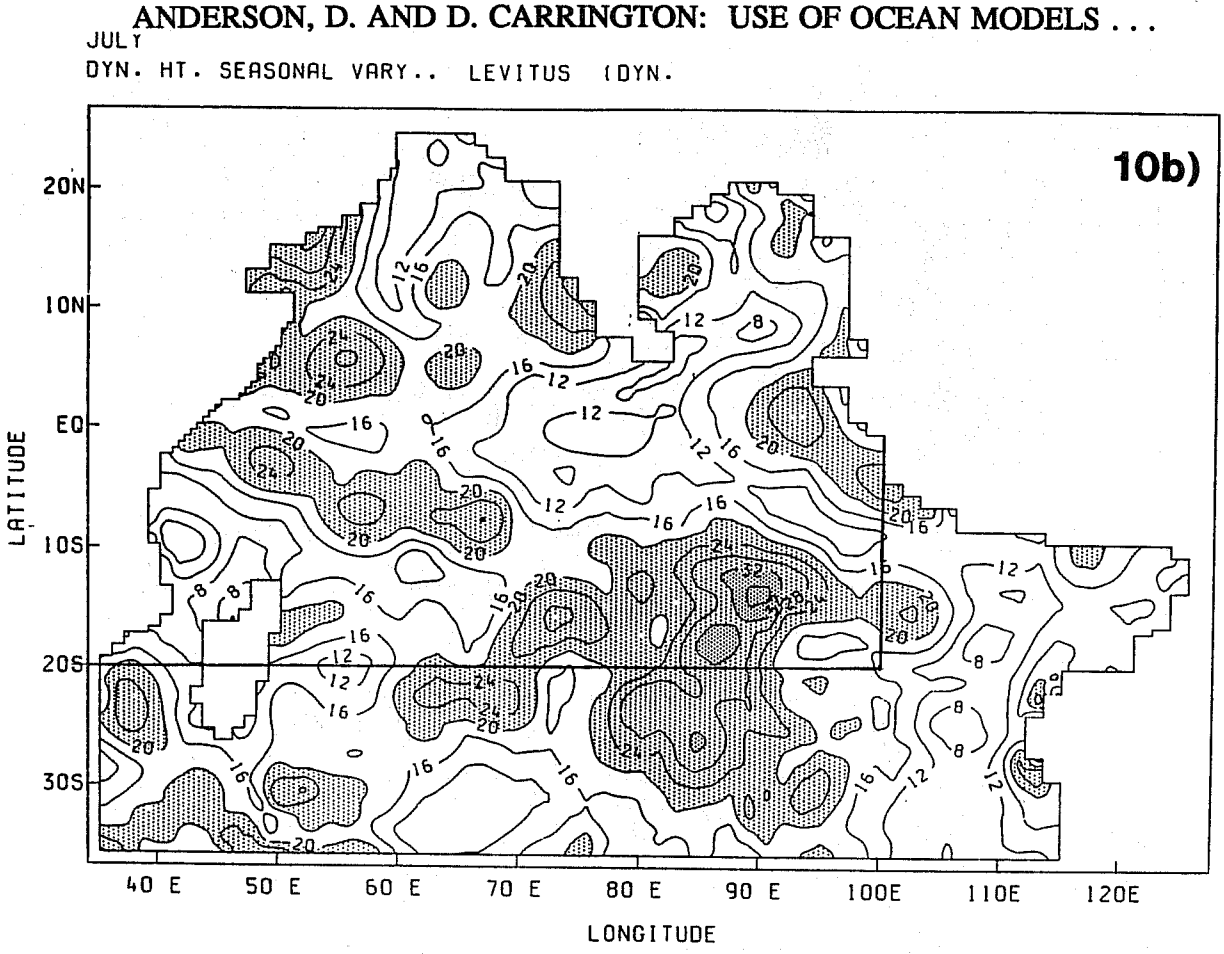
JULY
DYN. HT. SEASONAL VARY.. LEVITUS (DYN.
10b)
20N
10N
EQ
10S
20S
30S
LATITUDE
40 E
50 E
60 E
70 E
80 E
90 E
100E
110E
120E
LONGITUDE

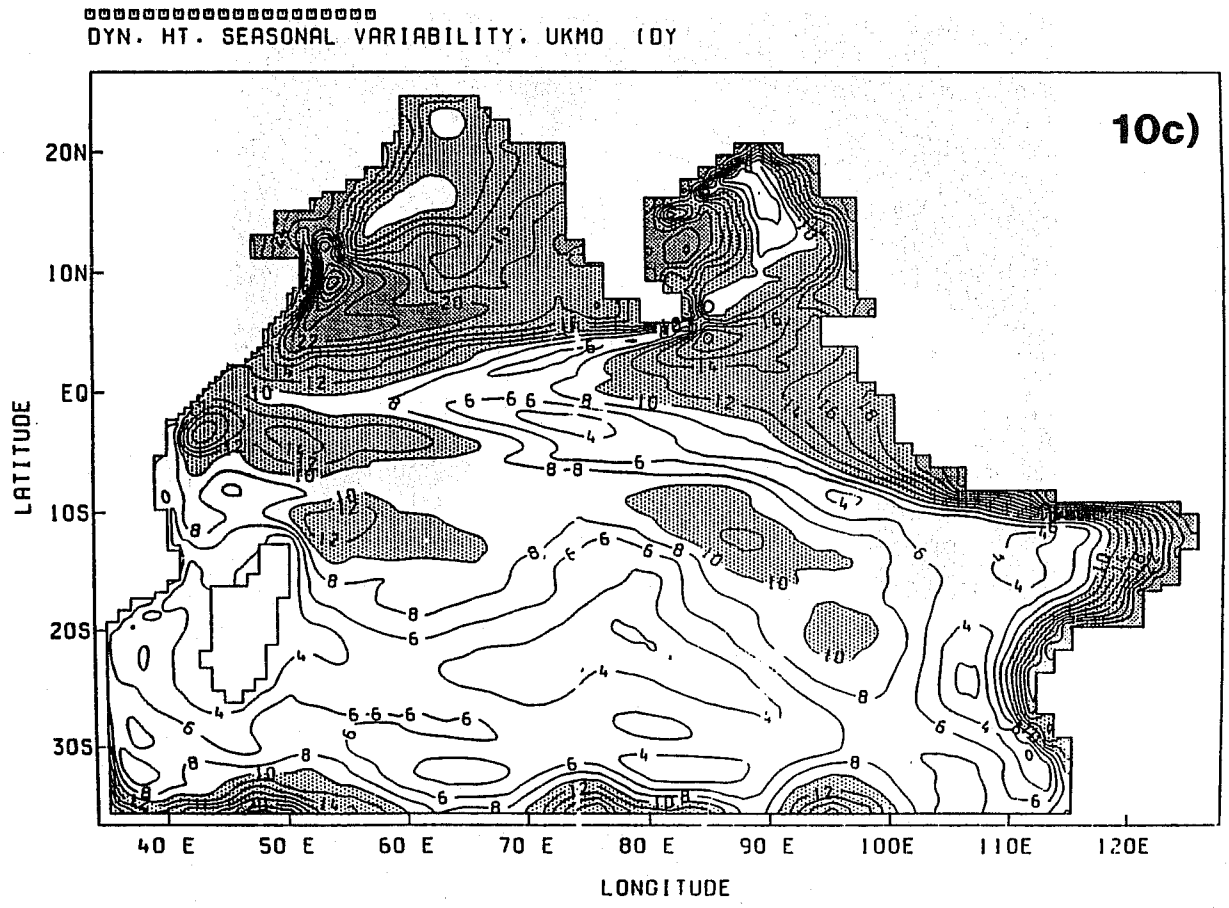
DYN. HT. SEASONAL VARIABILITY. UKMO (DY
10c)
20N
10N
EQ
10S
20S
30S
LATITUDE
40 E
50 E
60 E
70 E
80 E
90 E
100E
110E
120E
LONGITUDE

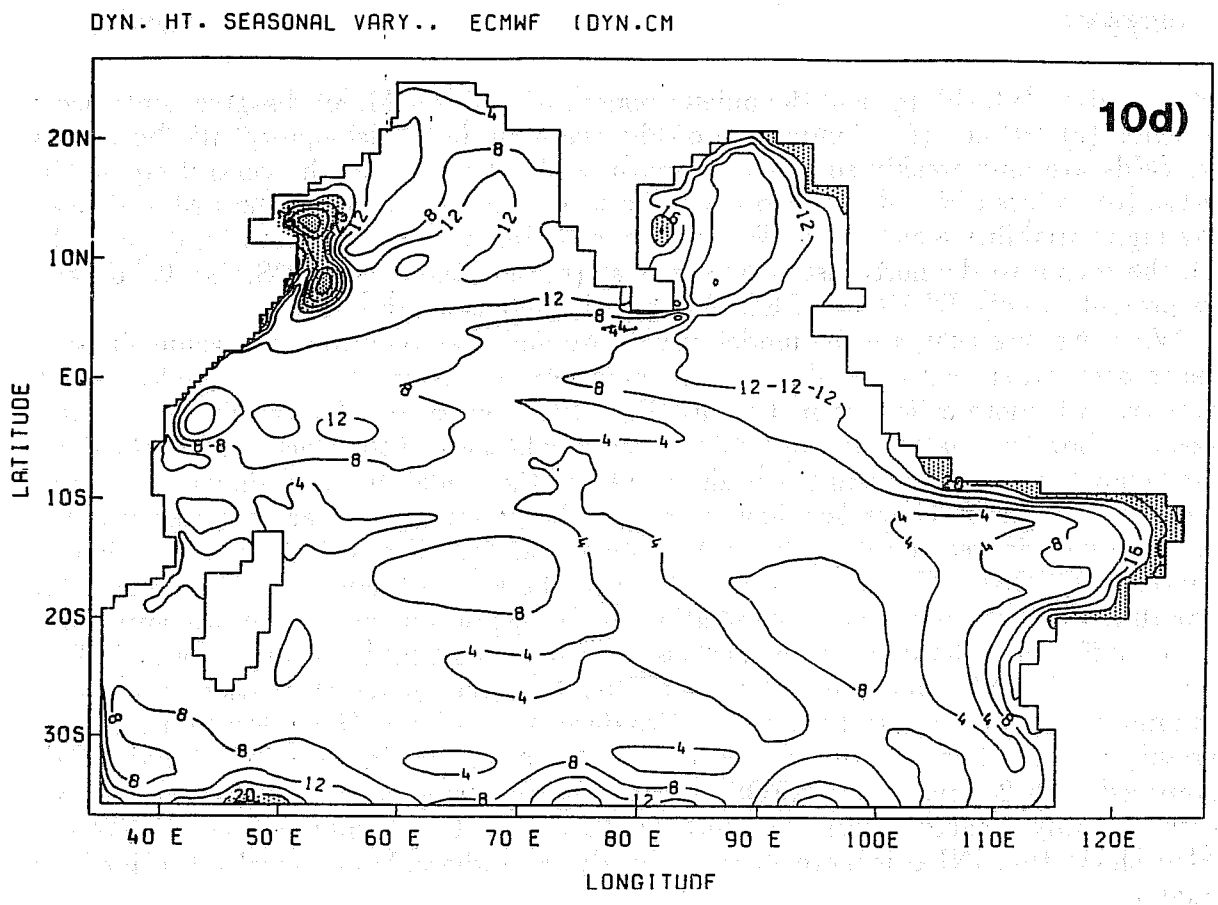
DYN. HT. SEASONAL VARY.. ECMWF (DYN.CM
10d)
20N
10N
EQ
10S
20S
30S
LATITUDE
40 E
50 E
60 E
70 E
80 E
90 E
100E
110E
120E
LONGITUDE

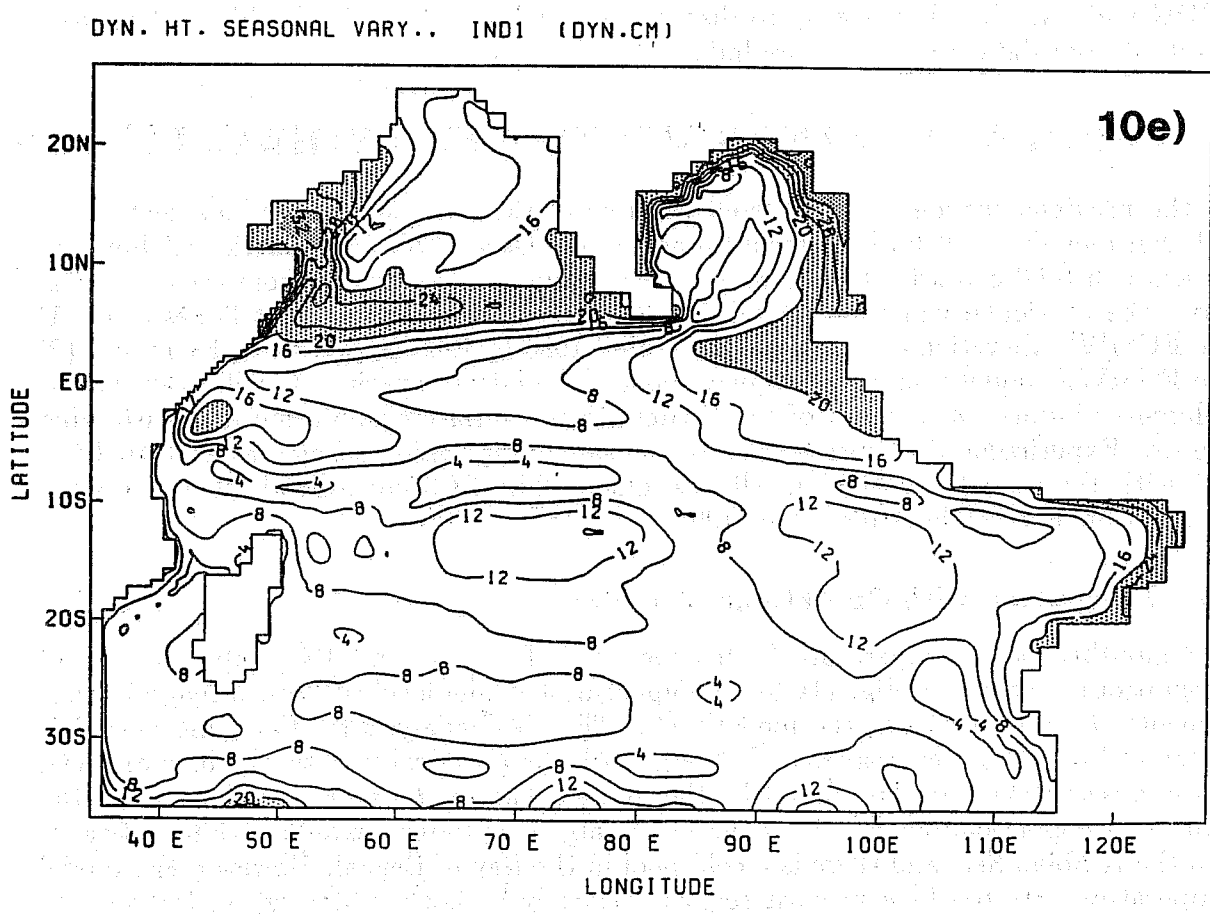
DYN. HT. SEASONAL VARY.. IND1 (DYN.CM)
10e)
20N
10N
EQ
10S
20S
30S
LATITUDE
40 E
50 E
60 E
70 E
80 E
90 E
100E
110E
120E
LONGITUDE

active regions (a), (b), (g) and the quieter regions (i) and (e). Major disagreements occur in region (c), (d) and (f). Comparison of Fig. 10a with the model equivalents shows that the fields are only weakly similar over much of the domain. In the central equatorial region (e), values of 6–8 dyn cms occur in both, with higher values to the east and west. The high variability regions – the Western Arabian Sea, with a band from Kenya to India (a), the region to the northeast of Madagascar (h), and the region 10°S, 80–100°E (g) – are present in both INDG and GEOSAT, but the details are different.

When we intercompare the model results, we find that they too have some similarities to each other. All three show a maximum from the equator, 40°E extending south eastward (c), more or less as in Levitus (Fig. 10b), but of smaller amplitude. Levitus does not show the coastal high variability, probably because of the smoothing in the data. The behaviour in the Arabian Sea is also similar in the model runs and similar to Levitus although INDN is much weaker than observed. The (relatively) low activity region in the central equatorial region (e) is present in all models and smaller in the model runs than in Levitus or GEOSAT. One of the main differences between all figures is in the region (g) near 10°S where the models and observations both suggest a maximum but the amplitude is very different: ~36 dyn cms in Levitus, 32 cms in GEOSAT, 10 dyn cms in INDG, 12 dyn cms in IND1 and 6 dyn cms in INDN. All three model calculations indicate a maximum along the eastern boundary not confirmed by either of the observed fields. The variability in the Somali gyre reaches 32 dyn cms in the model runs INDG and INDN compared with 20 cms in the GEOSAT data. Levitus does not show this feature well, again probably because of coastal smoothing of the data. Comparison between INDG and INDN shows that INDG is more energetic nearly everywhere, but especially South of the equator.

The conclusion from this section is that while there are significant differences between INDG and INDN, it is not easy to discriminate and say one is preferable, largely as a result of poor data coverage in the Indian Ocean region.

4 USING AN OCEAN MODEL TO 'VERIFY' HEAT FLUXES

In the previous section we considered the role of the wind stress. In this section we will consider fluxes of both momentum and heat. Ocean SST is a function of both, so an error in SST can arise from errors in momentum flux as well as from errors in heat flux. The particular examples we will consider are the stresses and heat fluxes from (1) the ECMWF operational system for the period 1985 to 1988 (Experiment EC1) and (2) the ECMWF model running in climate mode. The latter experiments will examine the differences induced as a result of the changes to the surface evaporation at lowish wind speeds. Experiment EC2 corresponds to the same evaporation scheme as used in EC1, but with the model now used in climate mode while EC3 corresponds to the revised formulation as given by Miller *et al.* 1992.

4.1 Integration with Operational Analyses

The monthly-mean temperature from experiment EC1 for July 1988 (after 1 year of integration) is shown in Fig. 11a for the uppermost model level (0-10m, which will subsequently be referred to as the model SST). The CAC analysis for the same period is shown in Fig. 11b for comparison. The large-scale geographical variations which are seen in the observations are reproduced by the model. The temperatures are highest in the equatorial region and north of the equator. A large cold tongue extends north-eastwards into the Arabian Sea, and there is a cold pool in the Bay of Bengal. However, the model temperatures are too high in most regions, typically by 2-3°C, although in the eastern equatorial region they are 6-7°C too warm. In contrast, the model temperatures are colder

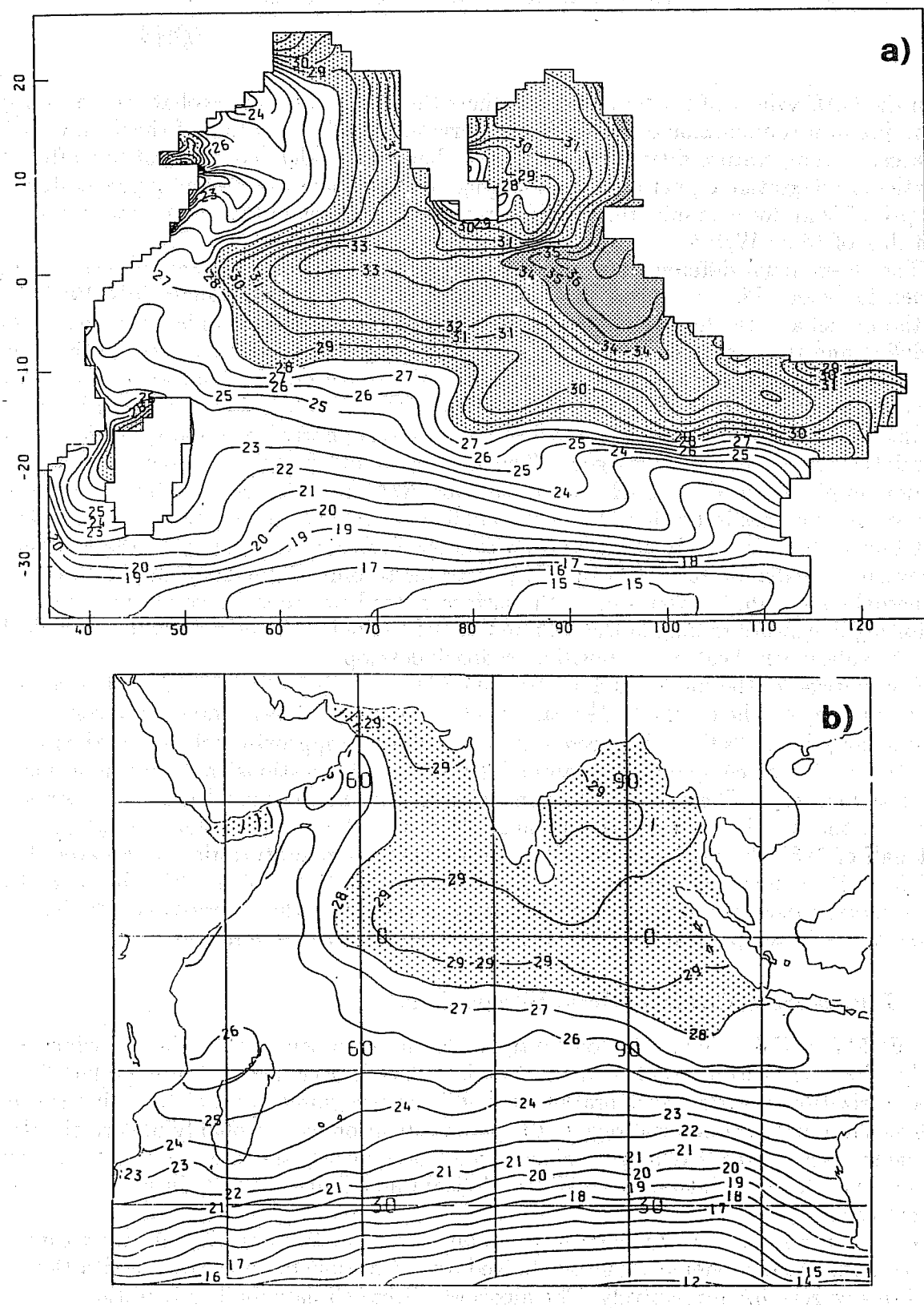

Figure 11: Sea surface temperatures (°C, monthly average) for July 1988 a) for experiment EC1 and b) CAC 2° x 2° analyses. (Temperatures greater than 28°C are shaded and temperatures greater than 34°C are heavily shaded.) The qualitative patterns are similar in a and b, but the model values are generally too high, particularly in the equatorial region.

than the CAC values off the Somali coast where the CAC values are probably erroneously high, due to a combination of insufficient observations and smoothing of the data into 2° squares. A temperature difference of only 2-3° between model and observations after 12 months of integration is, perhaps, encouraging. If this amount of warming penetrated to a depth of 50m, for example, this would correspond to a bias in the annual mean surface heat flux of 15-20 W/m^2.

The interannual differences seen in the observations are not well reproduced by the model, however. Fig. 12 shows the difference in SST, July 1988 minus July 1987, (a) for the model and (b) for the CAC analyses. There is some weak similarity between the modelled and the observed patterns. For example 1988 is warmer than 1987 both in the east equatorial region and also in the region to the south east of Madgascar, and 1988 is cooler in both at 10°S, 70-80°E. However, there are also a number of regions in which the interannual differences in the model SST's are not supported by the observations, and overall the agreement is not very good. The interannual differences are also of considerably greater amplitude in the model than in the observations. This is probably a reflection both of inaccuracies in the fluxes and the manner of response of the model. The greater heat flux in 1988 is mostly taken up in a shallow surface layer, mainly in the top 50m; the warmest water in July 1988 (37°C) penetrates to only about 20m. If the heat flux is anomalously high, the warming of the surface water helps to stabilise the upper levels, inhibiting downward mixing of the heat and further reducing the depth of the layer which absorbs subsequent heat; i.e. a positive feedback develops.

Comparison of the modelled and observed SST's on the equator at 72°E (the central Indian Ocean) for the complete $3\frac{1}{2}$ years of integration (not shown) indicates a somewhat greater range in SST's than that seen in the observations, (approximately 6°C in the model over this period as compared with around 2°C in the observations) both intraseasonally and interannually. The sign of interannual differences in the model does not correlate well with the (much weaker) interannual signal in the observations. For example, in the first half of 1988 the model shows a large and steady temperature rise (of greater than 4°C from December 1987 to May 1988), whereas in the first half of 1987 the modelled temperature change is much more erratic; this contrasts with the observations which show a steady rise in temperature in 1987 and a more erratic evolution in 1988.

4.2 Fluxes from Climate Mode Integrations

The ECMWF NWP model is constantly under development. One change which directly affects the estimates of ocean surface heat flux is a change in the boundary layer parametrization of surface evaporation. It had been recognised that, at low wind speeds such as those in the equatorial region, the parametrization used probably underestimated the value of the surface exchange coefficient and consequently the latent heat flux. A new scheme was therefore introduced (Miller, Beljaars and Palmer, 1992) in an attempt to correct this.

To test the impact of this change in parametrization, two experiments were carried out with the ocean model using fluxes derived from atmospheric integrations with the old and the new schemes respectively. The fluxes were from climate mode integrations rather than from operational mode integrations, in order to have a control run ('old' scheme) for comparison. In this case the atmospheric model is integrated forward in time with no inputs after the initialisation at the start except for the lower boundary condition in which the sea surface temperatures are prescribed. This is in contrast to operational mode integrations in which atmospheric observational data are assimilated into the model every 6 hours. The atmospheric model state is therefore less constrained in climate mode than in operational mode. The ocean model experiment with the fluxes from the old boundary layer parametrization scheme will be referred to as EC2, and the experiment

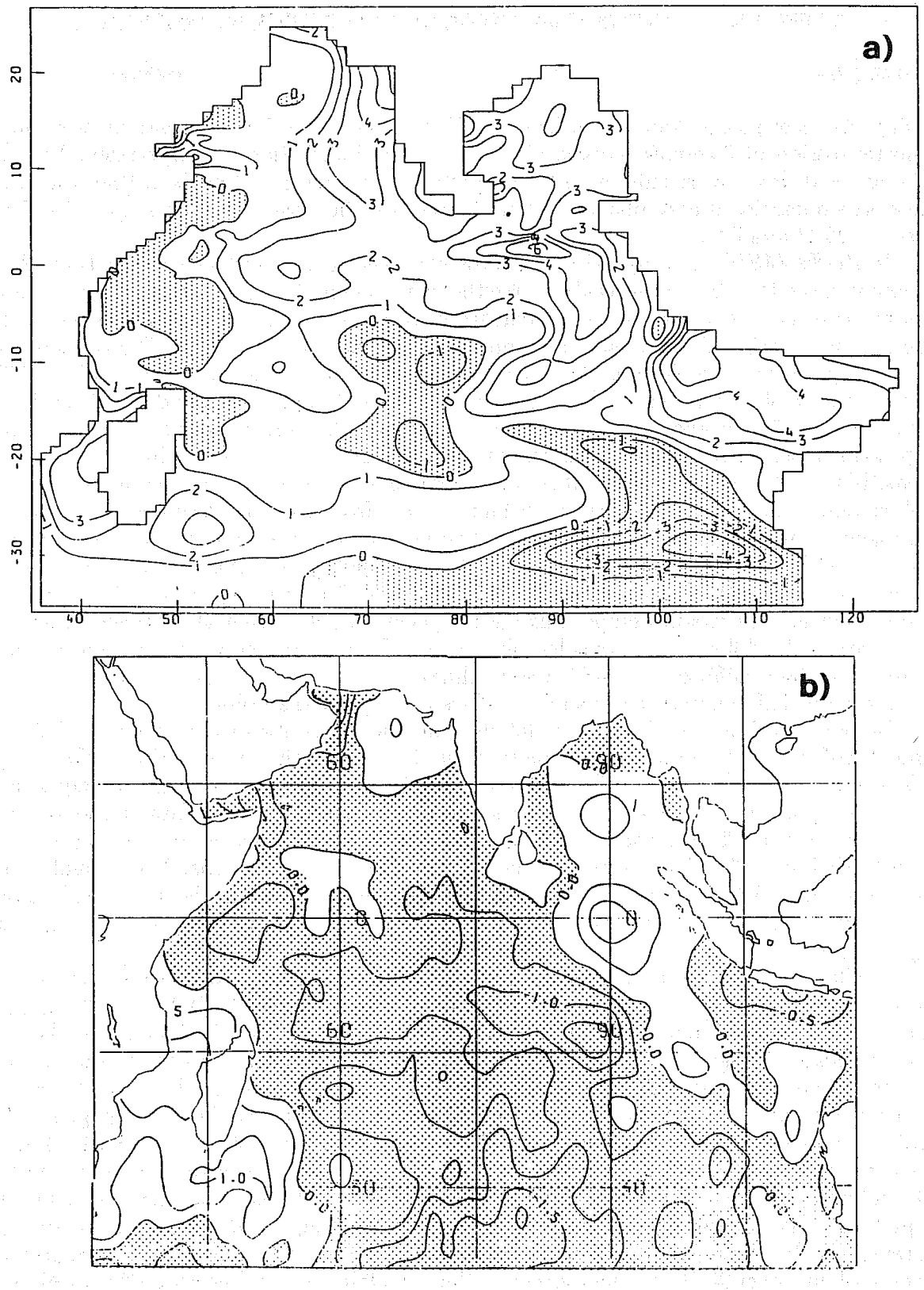

Figure 12: Interannual difference in sea surface temperature (°C, monthly average), July 1988-July 1987, a) for experiment EC1 and b) CAC 2° x 2° analyses. (Contour interval: 0.5°C. Negative values are shaded.) Some similar features can be seen in a and b, for example maxima around 90°E on the Equator and in the vicinity of Madagascar, but overall the correspondence between the modelled and observed interannual differences is low.

using the new parametrization scheme as EC3. These parallel integrations were for a shorter period of 3 months compared to the 1-year integrations in experiment EC1, as the fluxes differed more substantially from what the ocean model needed, than did those from the operational assimilation system. Fluxes for the period June to August 1987 are used in EC2 and EC3.

In the ECMWF (atmospheric) model integrations, the sea surface temperature (SST) analyses from the CAC were used to force the lower boundary. In principle, if the fluxes of momentum, heat and, to a lesser extent, fresh water were accurate and the ocean model perfect, then it should be possible to reproduce these SST's. The CAC SST's averaged on a 2°x 2° grid, are therefore used for comparison with the ocean model simulations. The extent to which the model SST's differ from the CAC values is a function of both the quality of the fluxes and of the ocean model, and it can be difficult to partition the error. By running the ocean model with two flux parametrizations, it is possible to gauge the sensitivity of the ocean model, but it is not possible to give an accurate estimate of truth. When the ocean model is forced with fluxes taken from the climate mode integrations, in experiments EC2 and EC3, the SST's diverge from observational values more rapidly than in EC1. Fig. 13a shows the model SST at the end of August 1987 (after three months of integration) from experiment EC2; Fig. 13b shows the CAC SST's for the same month. The model temperatures are typically 1-2°C higher than observed and in some areas the difference is considerably greater. The eastern equatorial region is again a region of large differences, 3-4°C higher than observed. Parts of the Arabian Sea show even greater differences, with modelled values 6°C higher than observed.

In the experiment with the new latent heat flux paramatrization scheme (EC3) the model SST's at the end of August are typically 3°C cooler than in experiment EC2. Fig. 13c shows the difference in SST's (EC3 minus EC2) for this time. In the eastern equatorial region they are 4-7°C cooler in EC3 than in EC2. In the northern Bay of Bengal and Northern Arabian Sea, however, they are warmer in EC3, in places by as much as 9°C. South of about 10°S there is little difference between the simulations. The actual SST's in experiment EC3 are shown in Fig. 13d. They are now too cool in the equatorial region, typically by 1-2°C. In the northern Bay of Bengal and Arabian Sea they are too warm by up to 5-6°C.

The large differences in SST between the simulations in EC2 and EC3 reflects the size of the difference in heat and momentum flux produced by the ECMWF model simply from the change in boundary layer parametrization. The parametrization change has led to significant changes in the simulated circulation, such that the resultant surface flux changes far exceed those directly resulting from the parametrization. Fig. 14a shows the difference in latent heat flux, Fig. 14b the difference in solar heat flux, and Fig. 14c the difference in net heat flux between the ECMWF climate mode integrations with the new and the old parametrization schemes for July 1987 (monthly mean values). As expected the latent heat flux in the new scheme (positive out of the ocean) is greater over the equatorial region, typically by 40-60 W/m^2 but locally by up to 120 W/m^2. However, the latent heat flux decreases over much of the region between 20°S and 30°S, the maximum amount being over 80 W/m^2, and in the northern Arabian Sea and northern Bay of Bengal it has also decreased, by up to 100 W/m^2.

The solar heat flux (Fig. 14b) is different with the new scheme in broadly the opposite sense to the latent heat flux: where the latent heat flux is greater, the solar is usually less, with a maximum decrease of 140 W/m^2 in the western equatorial region. Changes in the solar heat flux are associated with changes in the simulated cloud. The solar heat flux is greater with the new scheme in the Arabian Sea and northern Bay of Bengal by up to 60 W/m^2, and also around 10°S by a similar amount. An increase in latent heat flux and a decrease in solar heat flux have the same effect in reducing the net downward heat flux (and vice versa). Hence the monthly mean net downward heat flux for July 1987

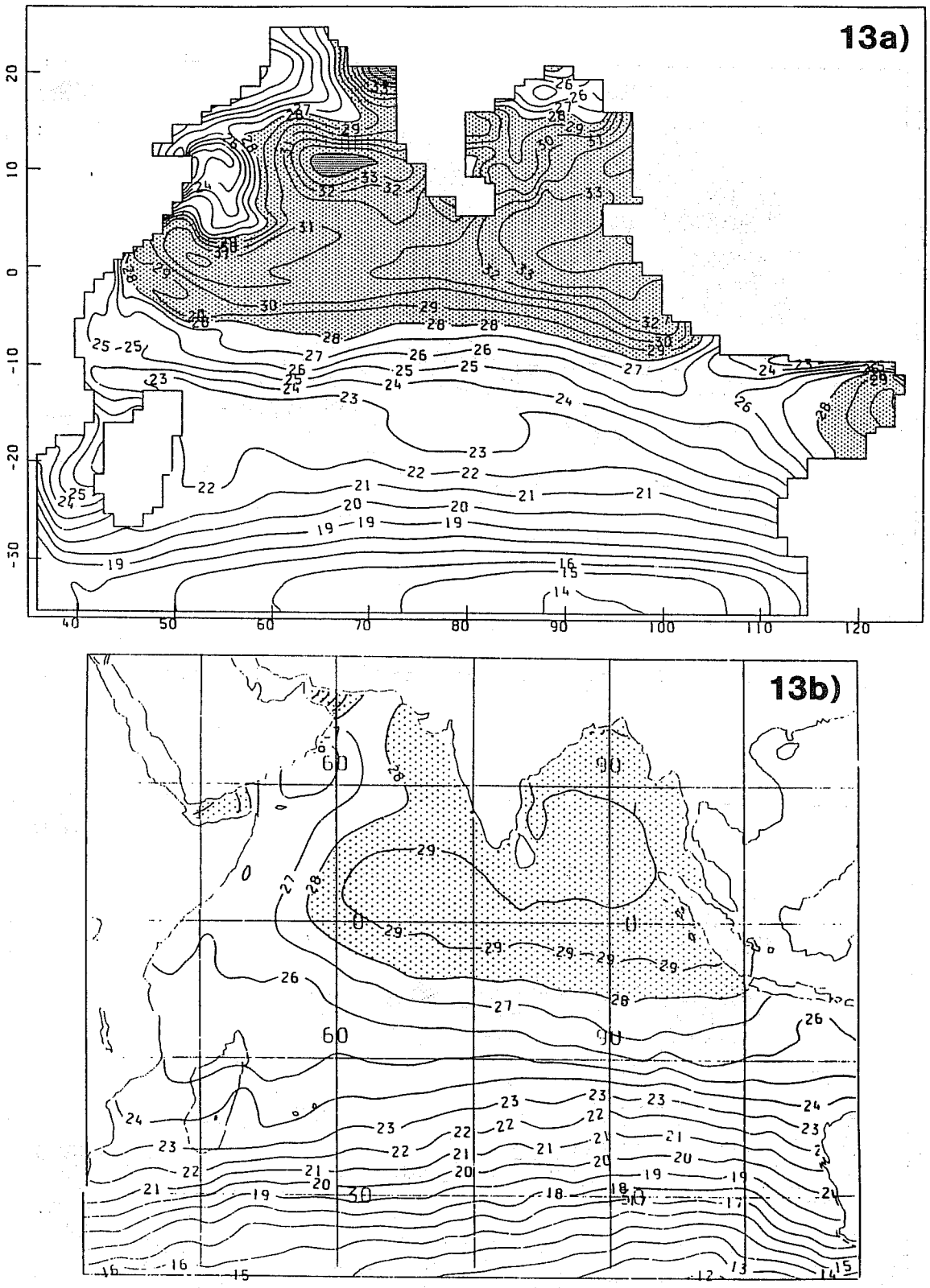

Figure 13: Sea surface temperatures for August 1987 (°C, monthly average): a) for experiment EC2; b) CAC 2° x 2° analysis; c) difference between experiment EC2 and EC3 (EC3-EC2); d) for experiment EC3. The different heat fluxes used in experiments EC2 and EC3 produce large differences in SST's. The SST's in the equatorial region are too warm in EC2 but too cool in EC3. The high temperatures in the northern Arabian Sea in EC2 are exagerrated further in EC3. In the Bay of Bengal, the wind field is displaced equatorward in EC3, leading to reduced evaporation there and strong warming as the solar flux is also increased. The spatial patterns of SST are, in general, correctly simulated by the model. The cold tongue off the Somali coast seen in the model fields, but not in the observations is probably qualitatively realistic.

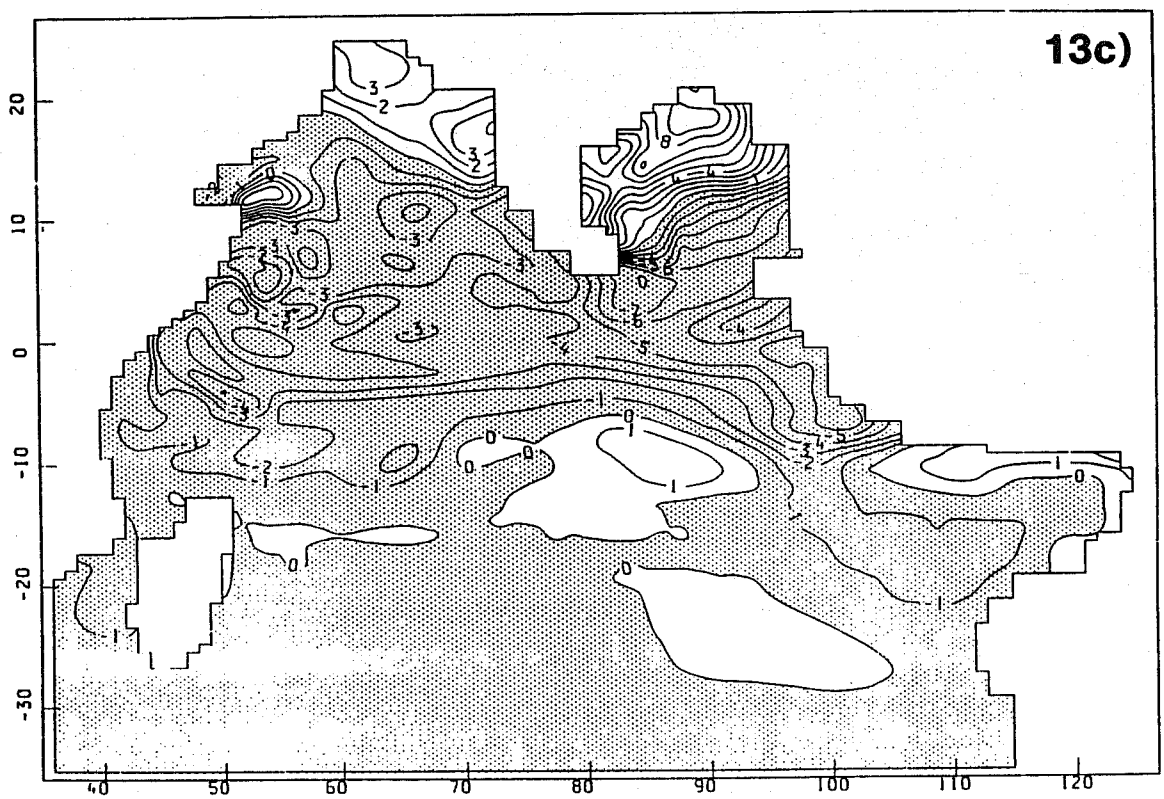
13c)
20
10
0
-10
-20
-30
40
50
60
70
80
90
100
110
120

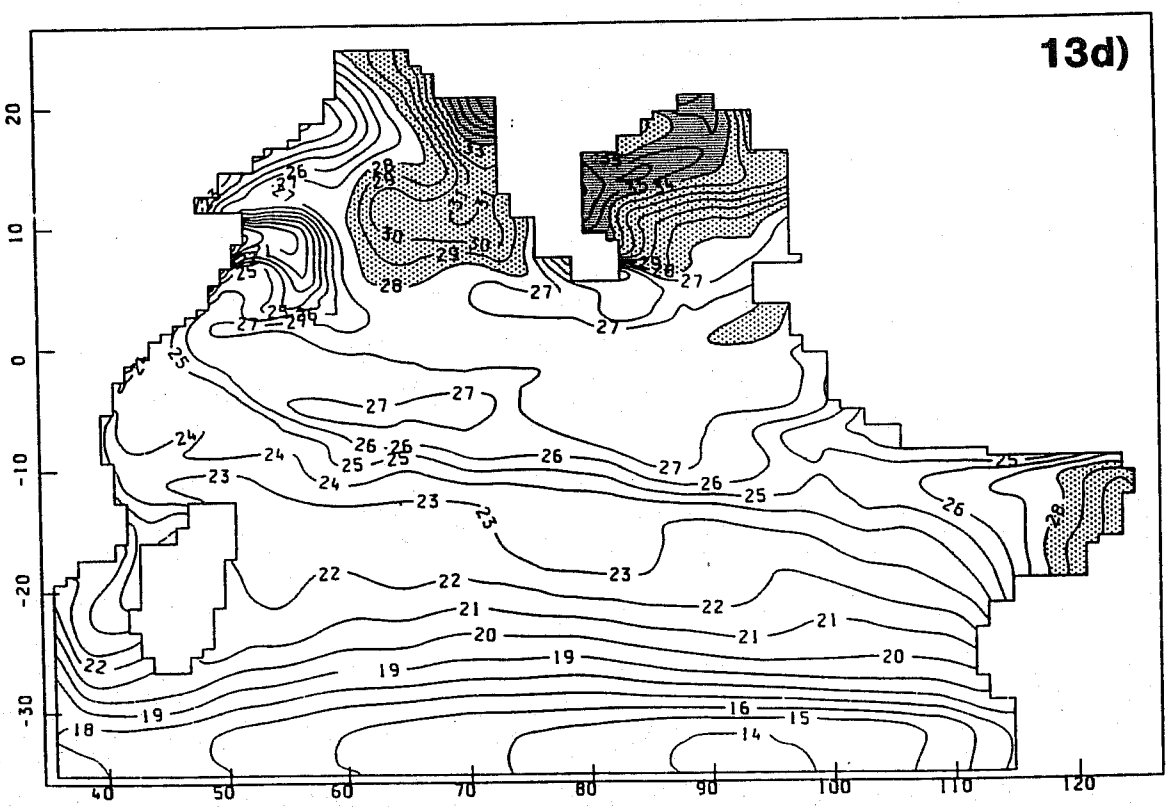
13d)
20
10
0
-10
-20
-30
40
50
60
70
80
90
100
110
120

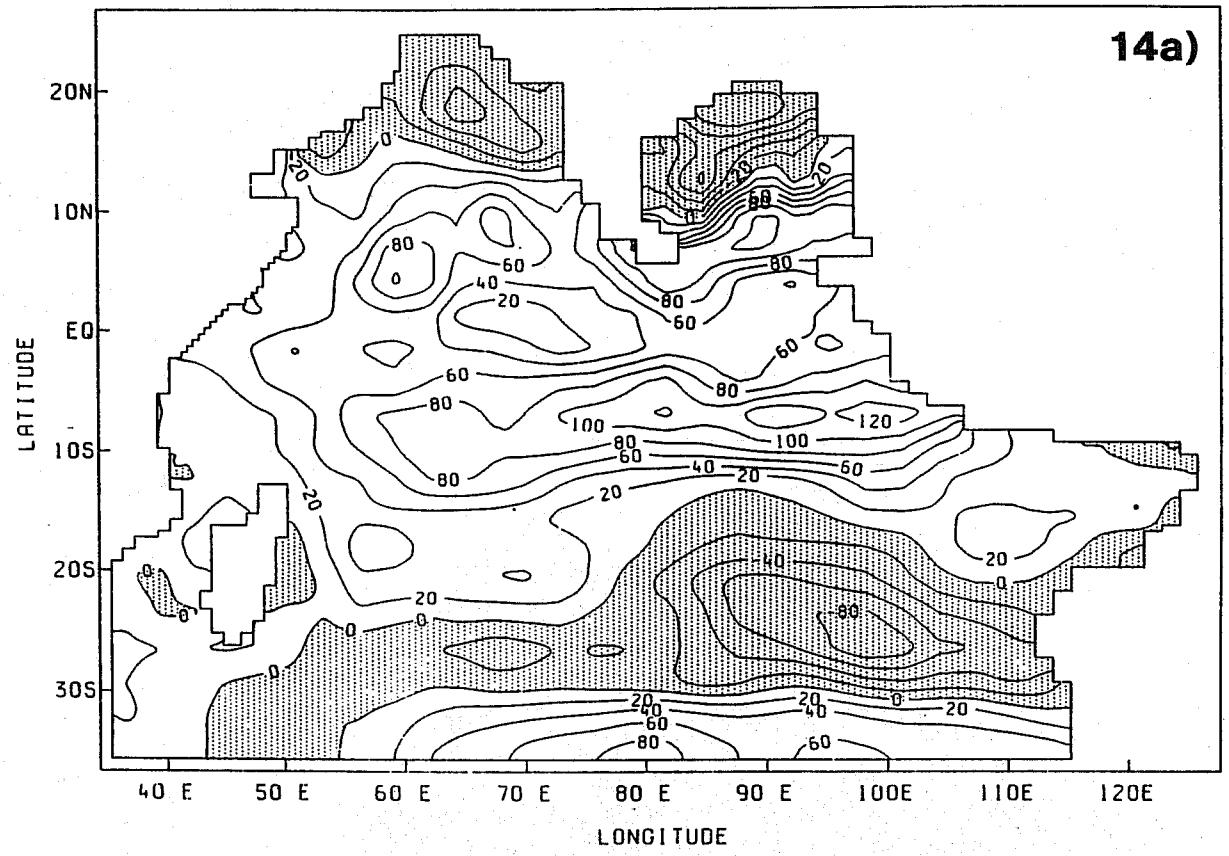
14a)
20N
10N
EQ
10S
20S
30S
LATITUDE
40 E
50 E
60 E
70 E
80 E
90 E
100E
110E
120E
LONGITUDE

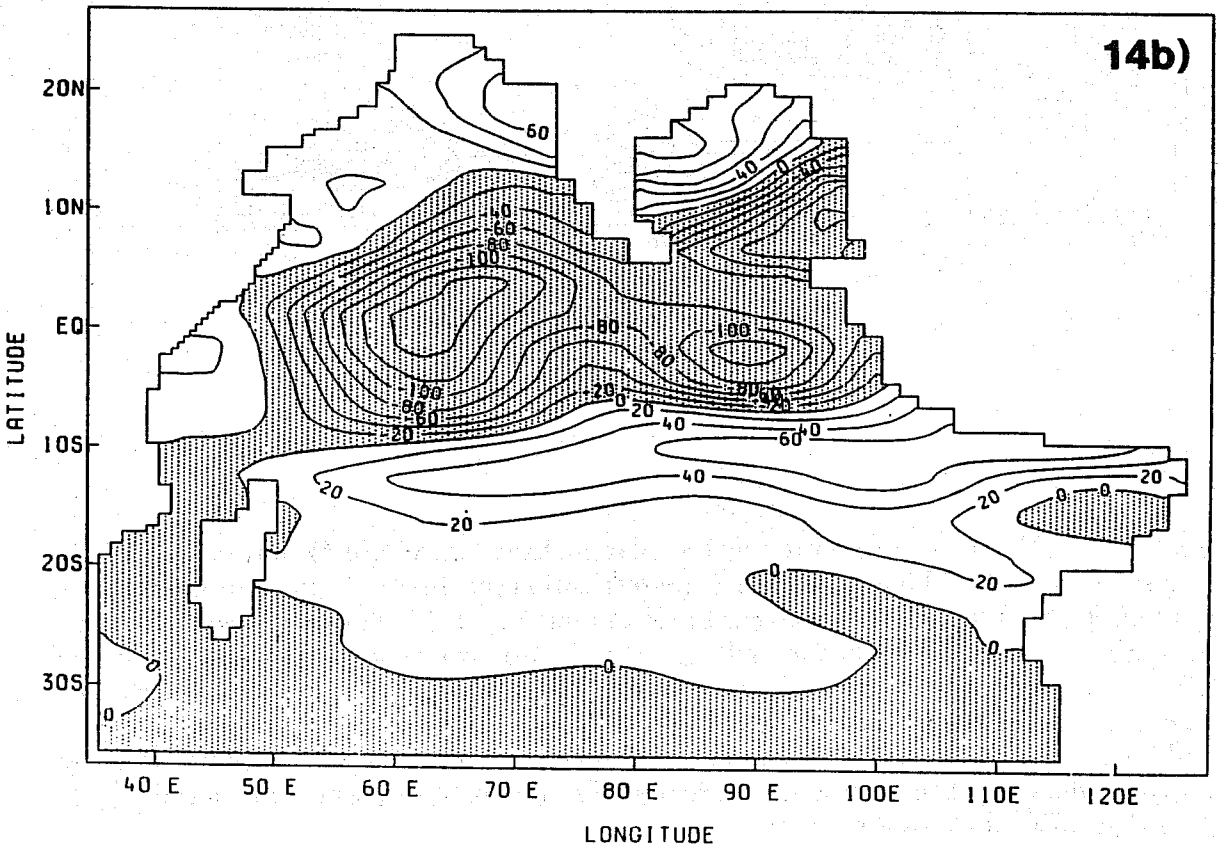
14b)
20N
10N
EQ
10S
20S
30S
LATITUDE
40 E
50 E
60 E
70 E
80 E
90 E
100E
110E
120E
LONGITUDE

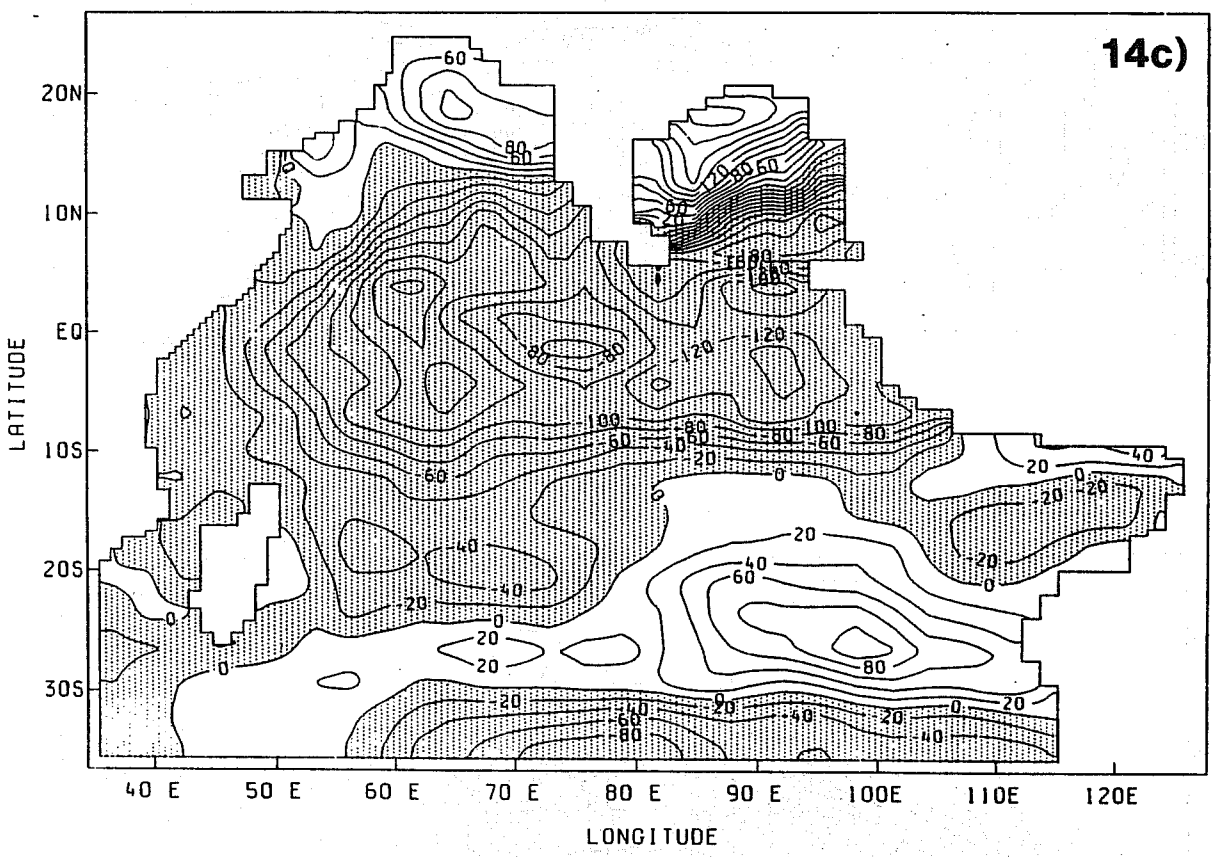

Figure 14: a) Difference in monthly average latent heat flux (W/m^2) between ECMWF integration with "new" boundary layer parametrization scheme (used in experiment EC3) and integration with "old" scheme (used in EC2) for July 1987. (Positive upward. Negative values shaded). b) As a but for solar heat flux. (Positive downward. Negative values shaded). c) As a but for net surface heat flux (latent, solar, longwave and sensible). (Positive values shaded.) Latent heat flux is considerably greater, and solar heat flux considering less, in the equatorial region in the integration with the new scheme, leading to a large reduction in the net surface heat flux. In the northern Arabian Sea and Bay of Bengal these differences are reversed.

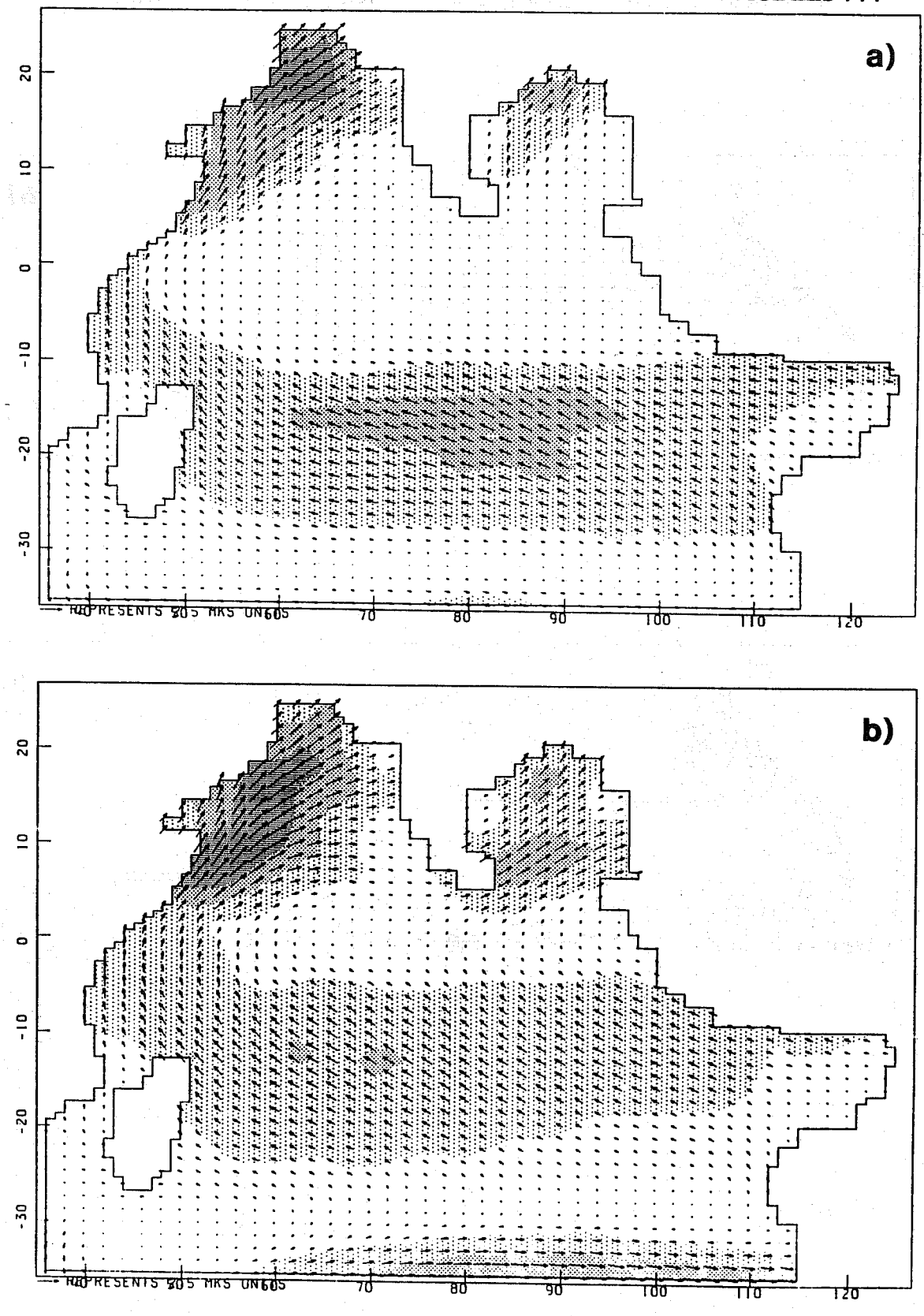

Figure 15: Wind stress vectors for July 1987 (monthly average) from the ECMWF integrations with a) the "old" boundary layer scheme (used in experiment EC2) and b) the "new" scheme (used in EC3). (Light shading: 0.075-0.15 N/m^2. Medium shading: 0.15-0.225 N/m^2. Heavy shading: $>$ 0.225 N/m^2) The wind stress is considerably enhanced with the new scheme in the equatorial region, and the regions of maximum wind stress have been shifted nearer to the Equator in both Northern and Southern Hemispheres.

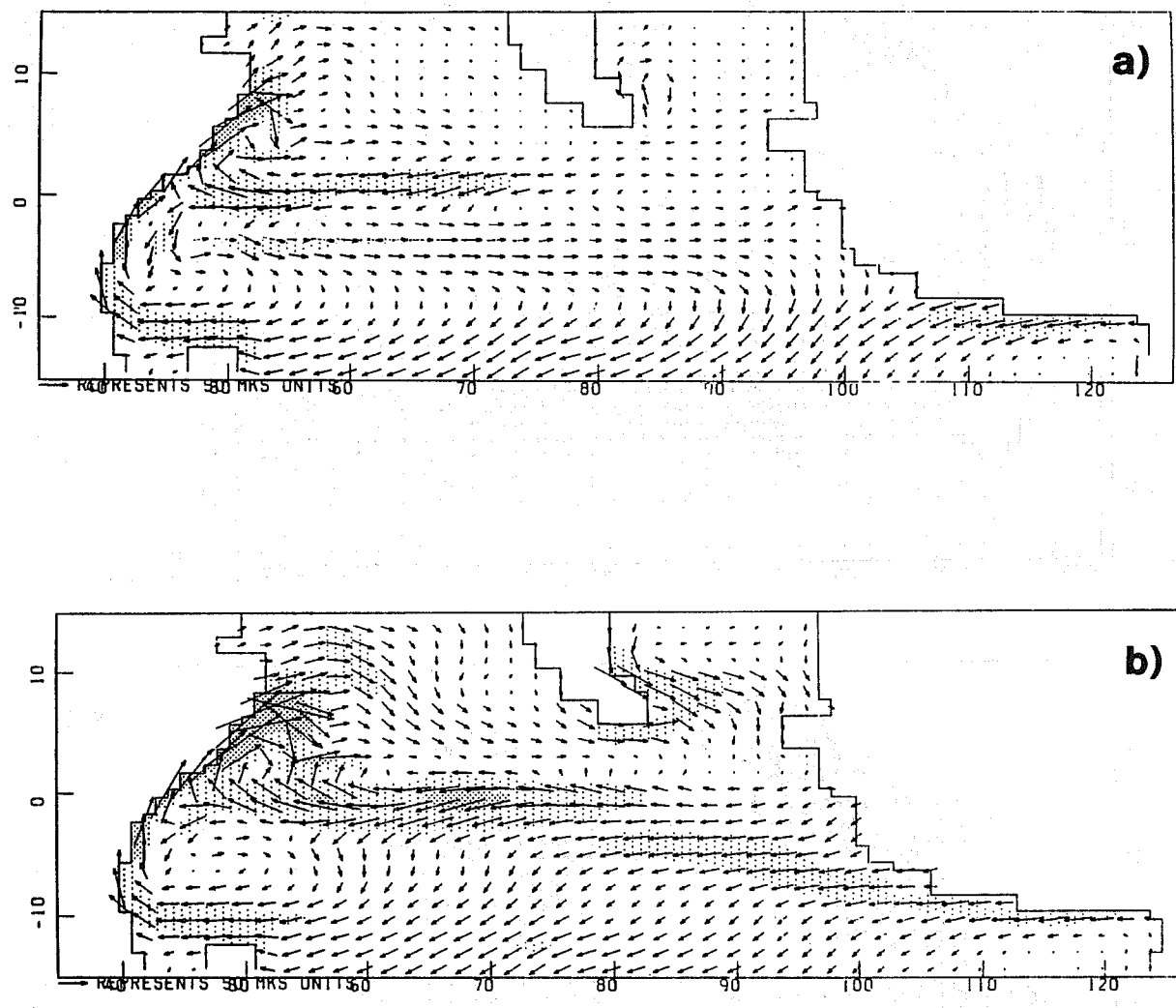

Figure 16: Surface currents (monthly average) for August 1987 from a) experiment EC2 and b) experiment EC3. (Light shading: 40-80 cm/s. Heavy shading: > 80 cm/s.) The currents in the equatorial zone, in the area east of Sri Lanka and in the Somali region are considerably stronger in b, reflecting the difference in wind stress (Fig. 15).

(Fig. 14c) is less with the new parametrization by up to 240 W/m^2 on the Equator and is greater by as much as 220 W/m^2 in part of the Bay of Bengal.

These changes in latent heat flux are a consequence of changes in the wind stress as well as in the parametrization. Fig. 15 shows the monthly mean wind stress for July 1987 with a) the "old" parametrization scheme and b) the "new" parametrization scheme. The areas of maximum wind stress are closer to the Equator in b) than in a), also being more extensive in b) in the Northern Hemisphere but more extensive in a) in the Southern Hemisphere. There is little difference between the peak maxima. Between 10°N and 10°S the circulation is considerably more vigorous in b). Immediately around the Equator the wind stress is near zero in a) but typically 0.025-0.05 N/m^2 in b). Between 20°S and 30°S the stress in b) is significantly weaker than in a), and it is also slightly weaker in b) in the northern Arabian Sea and northernmost Bay of Bengal, consistent with the latent heat flux changes discussed above. The overall impression is that there has been a distinct latitudinal readjustment of the wind patterns, which is likely to lead to a significant change in ocean circulation.

Fig. 16 shows the model surface currents for August 1987 north of 15°S for a) experiment EC2 and b) experiment EC3. The Somali gyre (around 5°N, 50°E) and the westward equatorial current are both considerably stronger in EC3. The eastward current at 5°S which extends across nearly the whole width of the basin in EC2 is replaced in EC3, east of 70°E, by a strong westward current. The main features of the surface circulation in EC3 are stronger than the August values of any year simulated by Anderson and Carrington (namely 1987-1990). They are also stronger than the August currents in the seasonal cycle simulation of Anderson *et al.* The undercurrent in EC3 is also stronger than any simulated for August in section 3 but it is of similar strength to that in the seasonal cycle simulation.

ACKNOWLEDGEMENT

The authors would like to acknowledge support of the NERC under grant GR3 7366 and the EC under contract EV4C.0042, and to thank Laury Miller for providing the GEOSAT data.

REFERENCES

Anderson, David L.T., D. Carrington, R. Corry and C. Gordon (1991). Modelling the variability of the Somali current J. Mar Res **49** 659-696.

Bell, R.S., and A. Dickinson (1987). The Meteorological Office operational numerical weather prediction system. Sci. Paper, Meteorological Office, No.41.

Blondin, C., and H. Böttger (1987). The surface and sub-surface parameterisation scheme in the ECMWF forecasting system. ECMWF Research Department Technical Memo No.135.

Burridge, D., and Gilchrist, A., (1989). Estimates of surface fluxes from global operational numerical weather predictions. Phil. Trans. R. Soc. Lond. **A329** *303-315.*

Esbensen, S.K., and Y. Kushnir (1981). The heat budget of the global ocean: An atlas based on estimates from surface marine observations. Report No. 29, Climate Research Institute, Oregon State University, Corvallis.

Hellerman, S., and M. Rosenstein (1983). Normal monthly wind stress over the world ocean with error estimates. J. Phys. Ocean, **13**, *1093–1104.*

Knox, R., (1976). On a long series of measurements of Indian Ocean equatorial currents near Addu Atoll. Deep Sea Res. **23**, *211–221.*

Latif, M., and A. Villwock (1990). Interannual variability in the tropical Pacific as simulated in coupled ocean-atmosphere models. J. Mar. Sys., **1**, *51-60.*

Leetmaa, A., and H. Stommel (1980). Equatorial current observations in the western Indian Ocean in 1975 and 1976. J. Phys. Ocean. **10**, *258–269.*

Levitus. S., (1982). Climatological atlas of the world ocean. NOAA Prof. Paper No.13. US Government Printing Office.

Miller, M., Beljaars, ACM and Palmer, TN., (1992). The sensitivity of the ECMWF model to the parametrization of evaporation from from the tropical oceans. J. Clim., *in press,*

Oberhuber, J.M., (1988). An atlas based on the COADS data set: The budgets of heat,buoyancy and turbulent kinetic energy at the surface of the global ocean. Max Plank Inst. fur Meteorologie Report No. 15.

Reverdin, G., (1987). The upper equatorial Indian Ocean: the climatological seasonal cycle. J. Phys. Ocean **17**, *903–927.*

Stockdale, T.N., Anderson D.L.T., Davey M.K., Delecluse P., Kattenberg A., Kitamura Y., Latif M., and Yamagata T. (1992) TOGA Numerical Experimentation Group Intercomparison of tropical ocean General Circulation Models (to be published)

Wyrtki, K., (1973). An equatorial jet in the Indian Ocean. Science **181**, *262–264.*